Removal of Hexavalent Chromium From Wastewater by Cu/Fe Bimetallic Nanoparticles

Jien Ye
Zhejiang University
Yi Wang
Zhejiang University
Qiao Xu
Zhejiang University
Hanxin Wu
Zhejiang University
Jianhao Tong
Zhejiang University
Jiyan Shi (shijiyan@zju.edu.cn)
Zhejiang University https://orcid.org/0000-0002-1601-8657

Research

Keywords: Nanoscale zerovalent iron (nZVI), Hexavalent chromium, Cu/Fe bimetallic nanoparticles, Reduction

Posted Date: December 11th, 2020

DOI: https://doi.org/10.21203/rs.3.rs-123533/v1

Removal of hexavalent chromium from wastewater by Cu/Fe bimetallic nanoparticles

Jien Ye [1,2], Yi Wang [1,2], Qiao Xu[1,2], Hanxin Wu[1,2], Jianhao Tong[1,2], Jiyan Shi [1,2]*

1 Department of Environmental Engineering, College of Environmental and Resource Sciences, Zhejiang University, Hangzhou 310058, China;

2 MOE Key Laboratory of Environment Remediation and Ecological Health, College of Environmental & Resource Science, Zhejiang University, Hangzhou 310058, China;

*Corresponding author

Jiyan Shi

Tel.: +86-571-8898-2019; Fax: +86-571-8898-2019; E-mail: shijiyan@zju.edu.cn

Abstract

Background: Nanoscale zerovalent iron (nZVI) is a promising material for removing heavy metals from wastewater. However, passivation of nZVI hinders its efficiency in water treatment. Loading another catalytic metal has been found to improve the efficiency significantly. In this study, Cu/Fe bimetallic nanoparticles were prepared by liquid-phase chemical reduction for removal of hexavalent chromium (Cr(VI)) from wastewater. Purpose of this study was to clarify the effects and mechanisms of Cu loading on the removal efficiency of Cr(VI).

Results: The results showed that Cu loading can significantly enhance the removal efficiency of Cr(VI) by 29.3% to 84.0%, and the optimal Cu loading rate was 3% (wt%). The removal efficiency decreased with increasing initial pH and Cr(VI) concentration. It was found that Cr(VI) removal followed a pseudo-first-order kinetic model. When the Cu loading rate was 3%, the initial

concentration of Cr(VI) was 100 mg/L, the observed first-order rate coefficient (k_{obs}) was 0.016 min^{-1} for Cu/Fe bimetallic nanoparticles at pH of 3.5, which was twice than that of nZVI (0.008 min^{-1}). X-ray photoelectron spectroscopy (XPS) analysis indicated that Cr(VI) was completely reduced to Cr(□) and precipitated on the particle surface as hydroxylated $Cr(OH)_3$ and $Cr_xFe_{1-x}(OH)_3$ coprecipitation.

Conclusions: In this study, it was found that the loading of Cu can significantly increase the specific surface area and the Cr(VI) remove efficiency of nZVI, and the removal efficiency decreases with increasing pH and Cr(VI) initial concentration. Therefore, Cu loading can alleviate the passivation of nZVI effectively and can be beneficial for the application of iron-based nanomaterials in remediation of wastewater.

Keywords: Nanoscale zerovalent iron (nZVI); Hexavalent chromium; Cu/Fe bimetallic nanoparticles; Reduction

1. Background

Chromium (Cr) is widely used in industry such as electroplating, leather tanning, and metallurgy [1, 2]. During these industrial activities, Cr is inevitably released into groundwater and surface water [3]. Once entering into the environment, Cr exists in two stable states: hexavalent chromium (Cr(VI)) and trivalent chromium (Cr(III)). Trivalent chromium is non-toxic and present mainly in forms of $Cr(OH)^{2+}$, $Cr(OH)_2^+$, and $Cr(OH)_3$ in the environment. Since positively charged $Cr(OH)^{2+}$ and $Cr(OH)_2^+$ can be absorbed onto the colloid and other media with negatively charged surface by electrostatic action, while $Cr(OH)_3$ itself exists as precipitation, the mobility of Cr(III) in the environment is weak [4]. Compared with Cr(III), Cr(VI) (mainly exists as $HCrO_4^-$ and CrO_4^{2-}) is known to be carcinogenic, mutagenic, and teratogenic, and much more mobile in the environment

[5, 6]. In order to minimize the harm of Cr(VI), reduction of Cr(VI) to Cr(III) is one of the most common methods [7, 8].

Nanoscale zerovalent iron (nZVI) is a promising material for removing heavy metals from wastewater and has been used for Cr(VI) treatment in groundwater [9-12]. Removal of Cr(VI) involves 1) adsorption of Cr(VI) on the nanoparticles' surface, 2) reduction of Cr(VI) to Cr(III), and 3) coprecipitation of Fe(III)-Cr(III) (oxy)hydroxides, as follows [13-15]:

$$3Fe^0 + 2CrO_4^{2-} + 16H^+ \rightarrow 3Fe^{2+} + 2Cr^{3+} + 8H_2O \quad (1)$$

$$3Fe^{2+} + CrO_4^{2-} + 8H^+ \rightarrow 3Fe^{3+} + Cr^{3+} + 4H_2O \quad (2)$$

$$xCr^{3+} + (1-x)Fe^{3+} + 2H_2O \rightarrow Cr_xFe_{1-x}OOH + 3H^+ \quad (3)$$

However, due to the high reactivity of nZVI, iron oxide film is easily formed on its surface which prevents the further contact with contaminants, especially in neutral and alkaline conditions[16, 17].

In recent years, loading another catalytic metal onto the surface of nZVI has been found to effectively alleviate the passivation of nZVI [17-19]. In bimetallic particles, the catalytic metal, such as Pd [20, 21], Ni [22, 23], and Cu [19, 24], can provide more reactivity sites and promote electron transfer on nanoparticles' surface. Zhou et al. proved that the introduction of Ni to nZVI could prevent the aggregation of nZVI and improve the Cr(VI) removal efficiency [25]. Hu et al. found that the loading of Cu could not only enhance the removal rate of Cr(VI) but also increase the thickness of the oxidation film and the oxidation state of iron, which meant higher removal capacity per unit weight of nZVI [26]. Recent studies have pointed out that 1) catalytic metals can enhance the oxidation of nZVI during the interaction with pollutants through the formation of galvanic cells; 2) catalytic metals can facilitate the generation of activated atomic hydrogens which lead to the enhancement of reduction of pollutants and corrosion of nZVI [27-29]. Therefore, to better understand the removal performance and mechanism of Cu/Fe bimetallic nanoparticles, the removal

of Cr(VI) by Cu/Fe bimetallic nanoparticles was investigated in this study.

Cu/Fe bimetallic nanoparticles were prepared by chemical reduction in aqueous solutions and their reactivity towards Cr(VI) in wastewater was examined. The main aims of this study were to (1) investigate the Cr(VI) removal efficiency by bimetallic nanoparticles at different experiment conditions; (2) clarify the removal mechanism of Cr(VI) by Cu/Fe bimetallic nanoparticles. Results of this study could provide a theoretical basis for the application of iron-based nanomaterials in environmental remediation.

2. Materials and methods

2.1 Materials and chemicals

Ferric chloride hexahydrate ($FeCl_3 \cdot 6H_2O$), iron powder (100 mesh), anhydrous ethanol and cupric nitrate ($Cu(NO_3)_2$) were purchased from Sinopharm Chemical Reagent Co., Ltd, Shanghai, China. Potassium borohydride (KBH_4) and polyvinylpyrrolidone (PVP, K29-32) were purchased from Aladdin Bio-Chem Technology Co., Ltd, Shanghai, China.

Hexavalent chromium wastewater was prepared by the extraction of soil sampled from a decommissioned chemical plant in Hangzhou, China (120°18’E, 30°22’N). After air-dried and sieved to less than 1 mm, the soil samples (50 g) were extracted by deionized water (1 L) for 18 h. The supernatant was then filtrated and stored as the Cr(VI) stock solution. Elemental concentrations of heavy metals were determined by an atomic absorption spectrometer (AAS, MKII M6, Thermo Electron, USA). The basic properties of the chromium wastewater (pH = 8.32±0.10) were shown in Table 1.

Table 1. The concentrations of heavy metals in chromium wastewater (mg L^{-1})

Cr(VI)	Total Cr	Pb	Cu	Cd
1453.7 ± 6.3	1453.8 ± 8.3	3.24 ± 0.08	0.12 ± 0.01	0.04 ± 0.01

2.2 Preparation of Cu/Fe bimetallic nanoparticles

The Cu/Fe bimetallic nanoparticles were prepared through a modified chemical reduction method reported before. [26, 30, 31]. Briefly, 1.35 g $FeCl_3 \cdot 6H_2O$ and 0.5 g PVP (K29-32) were dissolved in 100 mL ethanol-water solution (30% v/v) in a three-necked flask. After mechanical stirring under N_2 environment for 10 min, 100 mL 0.2M KBH_4 (dissolved in 1% NaOH) was added dropwise by a constant pressure separation funnel. Ferric ions were reduced to zero-valent iron by the following reaction:

$$4Fe^{3+} + 3BH_4^- + 9H_2O \rightarrow 4Fe^0\downarrow + 3H_2BO_3^- + 12H^+ + 6H_2\uparrow \quad (4)$$

After being washed with deionized water and anhydrous ethanol for three times, the iron particles were dispersed in 100 mL oxygen-free water. Then, the desired doses of 1000 mg L^{-1} $Cu(NO_3)_2$ solution (2.8, 8.4, 14.0, 28.0 mL) were added dropwise for the preparation of bimetallic nanoparticles with the corresponding copper loading rates (1%, 3%, 5%, and 10%). After mechanical stirring under N_2 environment for 30 min, the products were washed with anhydrous ethanol for three times. The nZVI and Cu/Fe bimetallic nanoparticles were sealed storage.

2.3 Characterization of Cu/Fe bimetallic nanoparticles

The morphology of nZVI and Cu/Fe bimetallic nanoparticles was characterized by transmission electron microscope (JEM 1200EX, Hitachi, Japan) operating at 200 kV. Gas absorption operation was carried out for the determination of particles' specific surface area in a surface area analyzer (Tristar II 3020, Micromeritics, USA). X-ray diffraction (XRD) was performed in a X-ray diffractometer (D/max-rA, Rigaku, Japan) with Cu Kαradiation (λ=0.154 nm). The scan range was set from 10° to 80° at 40 kV and 40kV. X-ray photoelectron spectroscopy was

operated on a X-ray photoelectron spectrometer (Escalab 250Xi, Thermo Fisher Scientific, USA) with 250 W Mg Kαradiation.

2.4 Batch experiments

Cr(VI) removal experiments were performed in 250 mL conical flasks with an oscillation frequency of 400 rpm. Each flask contained 0.01 g nZVI or Cu/Fe bimetallic nanoparticles and 100 mL Cr(VI) wastewater, which was diluted from the Cr(VI) stock solution (1453.7 mg L^{-1}). After 1, 2, 5, 10, 20, 30, 60 min of reaction, 2 mL solution was sampled and filtered through a 0.22 μm membrane filter. The concentrations of Cr(VI) in the solutions were determined using the diphenylcarbohydrazide method. The absorbance of Cr(VI)-diphenylcarbohydrazide product was measured on a UV-vis spectrometer (UV-1800, Shimadzu, Japan).

3. Results and discussion

3.1 Characterization of Cu/Fe bimetallic nanoparticles

The nZVI and Cu/Fe particles (50-100 nm in diameter) were found to be mostly spherical in shape and both aggregated as a chain-like structure in the TEM images (Fig. 1). The aggregation of particles can be mainly caused by the magnetism and electronic interactions between the metals [32]. The Brunauer-Emmet-Teller (BET) isotherm was used to determine the specific surface area of ordinary iron powder, nZVI and Cu/Fe bimetallic nanoparticles, respectively (Fig. 2). The results showed that the specific surface area of nZVI (9.07 m^2 g^{-1}) was much higher than that of ordinary iron powder (0.15 m^2 g^{-1}). Copper loading can further increased the specific surface area of nZVI fivefold to 45.92 m^2 g^{-1}. This indicated that loading of Cu significantly reduced the agglomeration of nZVI. As observed from the XRD patterns of nZVI and Cu/Fe bimetallic nanoparticles (Fig. 3), a diffraction peak occurred at 44.8° both in nZVI and Cu/Fe bimetallic nanoparticles, which

corresponded to the (110) facet of bcc iron [33]. In addition, other diffraction peaks between 30° and 40° was also observed in nZVI, indicating the oxidation of iron and the formation of iron oxide (FeO) crystalline phases in nZVI [34]. However, such diffraction peaks missed in Cu/Fe bimetallic nanoparticles (Fig. 3). Compared with nZVI, the stronger diffraction peak at 44.8° and lacking of peaks between 30° and 40° implied that loading of Cu on the surface of nZVI could effectively reduce the oxidation of iron.

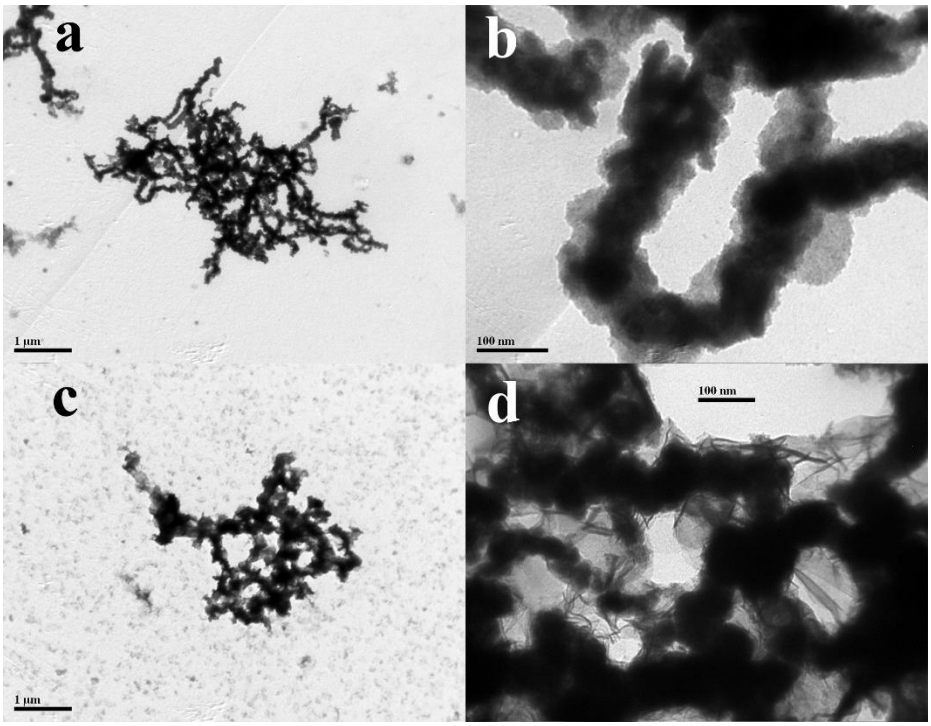

Fig. 1 TEM images of nZVI (a, b) and Cu/Fe bimetallic nanoparticles (c, d).

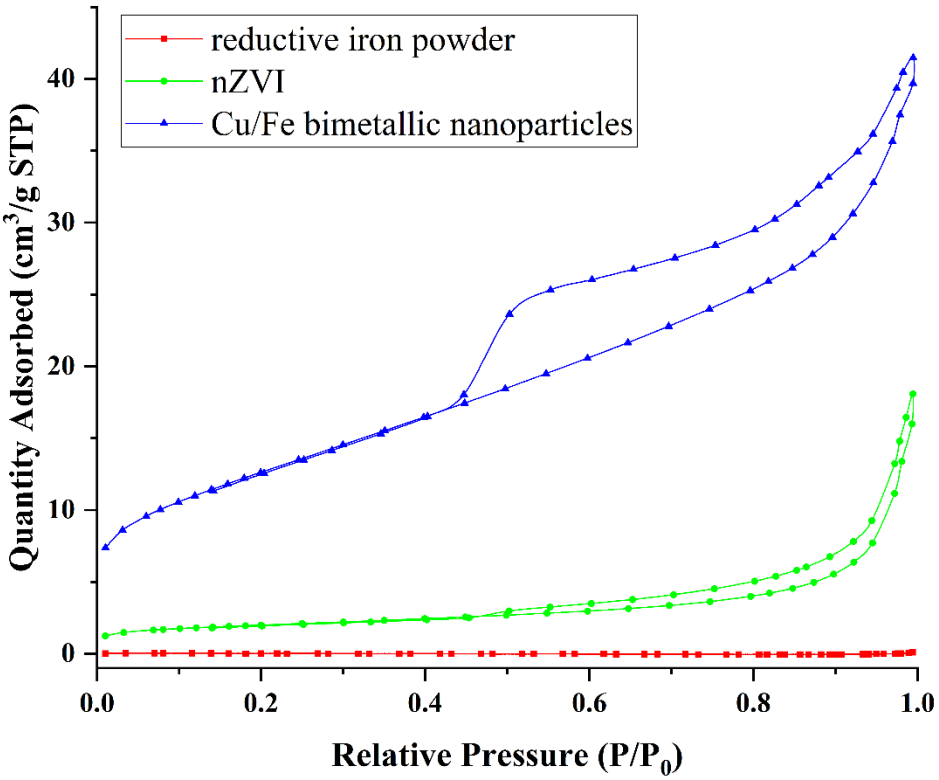

Fig. 2 The adsorption-desorption isotherms of reductive iron powder, nZVI, and Cu/Fe bimetallic nanoparticles.

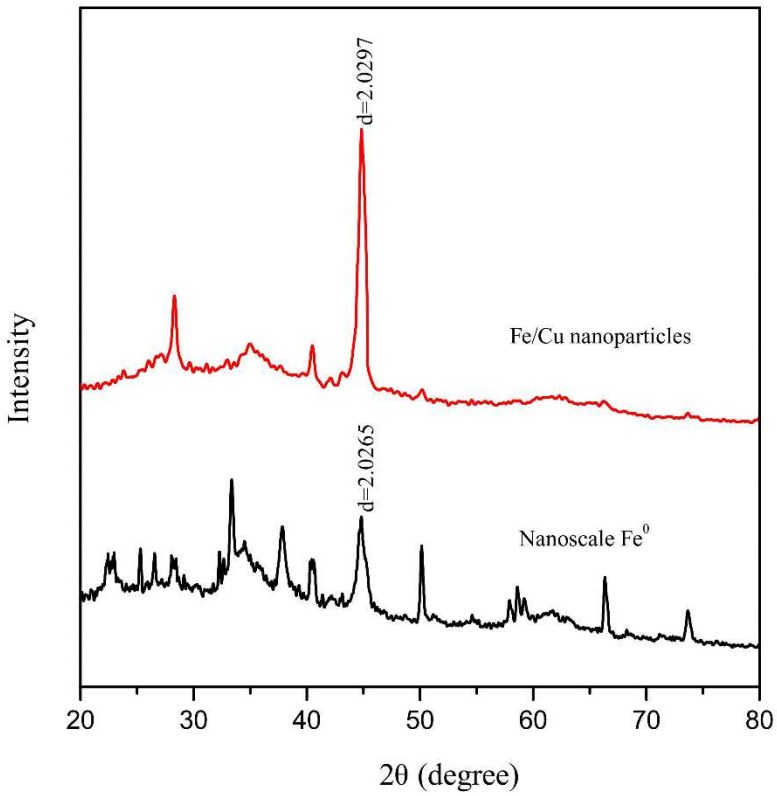

Fig. 3 XRD patterns of nZVI and Cu/Fe bimetallic nanoparticles.

3.2 Effect of Cu loading rate

The effect of Cu loading rates (1%, 3%, 5%, 10%) on the removal efficiency of Cr(VI) (100 mg L^{-1}) was investigated with batch experiments (Fig. 4). The Cr(VI) concentration decreased with increasing reaction time and the copper loading significantly increases the efficiency of Cr(VI) removal compared with nZVI. The removal efficiency of Cr(VI) increased from 37.47% to 48.46% and 68.94% after 60 min of reaction, respectively, as the Cu loading rate increased from 0 to 1% and 3%. Bransfield et al. found that for Cu loading below 1 monolayer equivalent (~ 10 μmol Cu/g Fe), the deposition of Cu occurred onto the iron surface. When the Cu loading was greater than 1 monolayer, Cu deposition occurred predominantly onto metallic copper that had already been deposited before[30]. Accordingly, the thickness of copper layer was assumed to increase linearly as the loading rates increased from 1% to 10% in this study. Due to the strong oxidizing ability of

Cr(VI), the metallic copper on the iron surface could be oxidized by Cr(VI) if the copper layer is not thick enough (equation (5)) [26].

$$3Cu + 2CrO_4^{2-} + 10H^+ \rightarrow 2Cr(OH)_3 + 3Cu^{2+} + 2H_2O \quad (5)$$

Therefore, an appropriate increase in Cu loading can enhance its catalytic ability. However, the removal efficiency of Cr(VI) declined as the Cu loading rate increased continuously to 5% and 10% (Fig. 4). This could be resulted from the aggregates of Cu nanoparticles and the shedding of Cu layer at the excessive Cu dosages [19, 35]. Studies showed that excessive Cu was easy to be dropped off from the iron surface by outside force (e.g., agitation or fluidization), which resulted in the loss of Cu catalytic ability [29].In addition, excessive Cu loading resulted in a decrease of the Fe hydroxide amount on the surface of the particles. Due to the strong adsorption capacity of Fe hydroxide, the decrease of Fe hydroxide reduced the adsorption capacity of the nanoparticles to Cr(VI), which consequently declined the Cr(VI) removal efficiency.

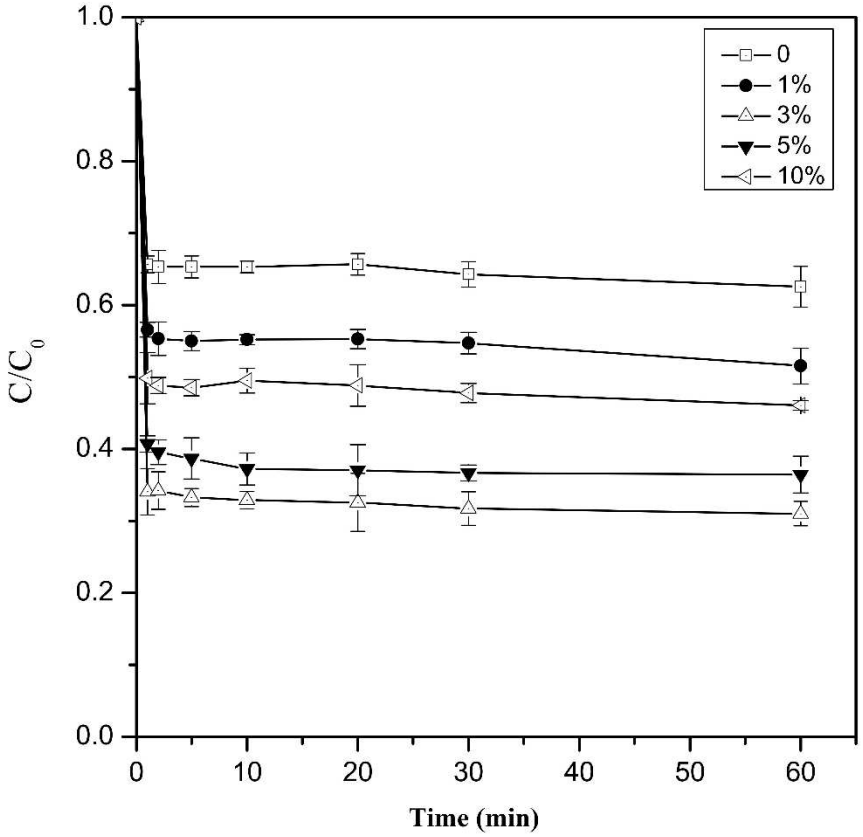

Fig. 4 Effect of copper loading rates on Cr(VI) removal by Cu/Fe bimetallic nanoparticles. Error bars indicate the standard deviation of the mean (n=3).

The Cr(VI) concentration in the wastewater decreased drastically in the first 2 minutes (Fig. 4). The reduction and removal of Cr(VI) by nZVI was carried out in two stages: 1) the Cr(VI) was firstly adsorbed on the particle surface of nZVI and 2) reduced then by internal electron transfer (Fig. 5). The redox reaction of Cu/Fe nanoparticles with Cr(VI) can be described by a pseudo-first-order kinetic model with a reaction rate proportional to the concentration of Cr(VI) in solution [36]:

$$\ln\left(\frac{C}{C_0}\right) = -k_{obs}t \quad (6)$$

where C_0 and C is the concentration of Cr(VI)initially and at different time, respectively. The k_{obs} (min^{-1}) is the observed first-order rate coefficiency.

The k_{obs} can be obtained by fitting $\ln(C/C_0)$ to the reaction time (Fig. S1, Table 2). When the

Cu loading rate increased from 0 to 1% and 3%, the k_{obs} increased from 0.0008 min^{-1} to 0.0009 min^{-1} and 0.0016 min^{-1}, respectively. As the loading rate increased continuously to 5% and 10%, the k_{obs}, however, decreased to 0.0015 min^{-1} and 0.0009 min^{-1}. This also agreed with the observation that the excessive Cu loading was not conducive to the reaction of nZVI with Cr(VI). The k_{obs} values obtained in this study were small compared with other studies [37, 38]. This may be because that the Cr(VI)-containing wastewater used in the present study was extracted from chromium-contaminated soil rather than formulated with potassium dichromate. Cr(VI)-containing wastewater contained other heavy metal ions such as lead, cadmium and copper, which could compete for reactive sites on the surface of nZVI [39]. Moreover, the solution pH was alkaline (pH = 8.32±0.10), which inhibited the reaction of Cu/Fe nanoparticles with Cr(VI) under high pH conditions [40].

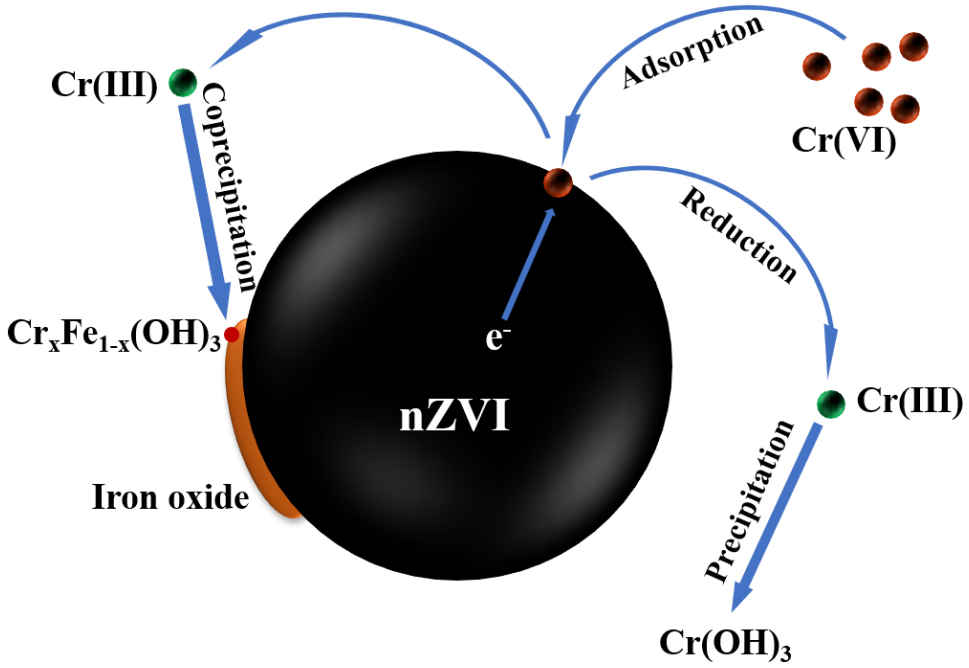

Fig. 5 Proposed mechanism for the removal of Cr(VI) using nZVI.

Table 2. Effect of copper loading rates on the kinetics of Cr(VI) reduction by Cu/Fe bimetallic nanoparticles

Cu loading rate (wt%)	k_{obs} (min^{-1})	R^2
0	0.0008	0.8673
1%	0.0009	0.8675
3%	0.0016	0.8882
5%	0.0015	0.5904
10%	0.0009	0.8518

3.3 Effect of initial pH

The removal efficiency of Cr(VI) by Cu/Fe bimetallic nanoparticles (3%) at initial pH of 3.5, 5.5, 8.5, 10.5 was investigated (Fig. 6). The removal efficiency of Cr(VI) was highest at pH of 3.5, reaching 69.40%, and slightly decreased to 61.65% and 63.23% when pH increased to 5.5 and 8.5, respectively. However, the removal efficiency of Cr(VI) decreased significantly from 69.40% to 55.34% as the pH increased from 3.5 to 10.5. This suggested that acidic conditions are more favorable for Cr(VI) removal by Cu/Fe nanoparticles. One possible reason is that under acidic conditions, the H^+ in solution can dissolve the iron oxide film formed on the surface of the nanoparticles according to the equation (3), which increased the exposure of the particle surface active site, thus improving the removal efficiency of Cr(VI). While under alkaline conditions, the OH^- in solution can react with iron to produce an iron oxide passivation layer covering the surface of the nanoparticles, occupying the particle surface active sites and inhibiting the reduction reaction [41]. In addition, the competition between OH^- and Cr(VI) species (CrO_4^{2-} and $Cr_2O_7^{2-}$) at alkaline conditions also suppressed the removal efficiency. Similarly, Mortazavian et al. (2018) also found that the removal of aqueous Cr(VI) by activated carbon supported nZVI also showed a higher efficiency at pH of 4.0 [42]. The authors explained that the increasing H^+ concentration allowed the reaction of the equations (1) and (2) to proceed to the positive direction, so that more Cr(VI) was

reduced to Cr(III).

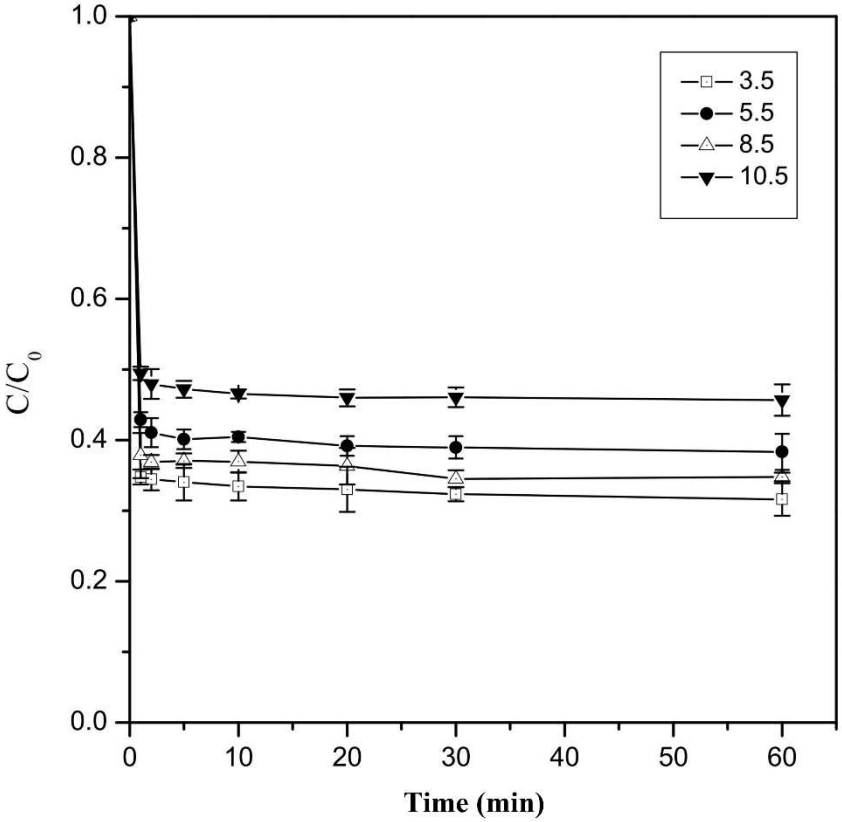

Fig. 6 Effect of initial pH on Cr(VI) removal by Cu/Fe bimetallic nanoparticles. Error bars indicate the standard deviation of the mean (n=3).

Similarly, the k_{obs} can be obtained by analyzing the relationship between $\ln(C/C_0)$ and reaction time under different initial pH conditions (Fig. S2, Table 3). It can be found that the k_{obs} decreased with increasing pH. The k_{obs} was 0.0016 min^{-1} when pH was 3.5, and the k_{obs} decreased to 0.0014 min^{-1} when pH increased to 5.5 and 8.5. When pH was 10.5, the k_{obs} decreased by 62% to 0.0006 min^{-1} compared to pH 3.5. The different reaction rates at the corresponding pH could be explained by the Cr(VI) speciation and the surface charges of the nanoparticles. At pH > 6.5, Cr(VI) speciation is predominantly CrO_4^{2-}, and at pH < 6.5, $HCrO_4^-$ is the dominant form. As the pH decreases, the reduction of hexavalent chromium becomes easier [25, 43, 44]. On the other hand, the pH of zero

point of charge (pH_{zpc}) for Cu/Fe bimetallic nanoparticles was measured to be 4.6 (see Fig. S4 in the Supplemental Information), which means that the surface of the Cu/Fe bimetallic nanoparticles is positively charged when the pH is less than 4.6. Therefore, at the initial pH of 3.5, there was an electrostatic attraction between the Cu/Fe bimetallic nanoparticles and $HCrO_4^-$, which allowed the Cr(VI) to be more easily adsorbed on the surface of iron particles and promoted the reduction rate [42, 45, 46].

Table 3. Effect of initial pH on the kinetics of Cr(VI) reduction by Cu/Fe bimetallic nanoparticles

Initial pH	k_{obs} (min^{-1})	R^2
3.5	0.0016	0.9003
5.5	0.0014	0.7459
8.5	0.0014	0.6523
10.5	0.0006	0.5770

3.4 Effect of initial Cr(VI) concentration

In this study, the removal of Cr(VI) was investigated at initial Cr(VI) concentrations of 50, 100, 150 and 200 mg L^{-1}, respectively, with Cu/Fe bimetallic nanoparticles (3%) applied at 0.1 g L^{-1} (Fig. 7). It can be found that the efficiency of Cr(VI) removal by Cu/Fe bimetallic nanoparticles decreased with the increase of the initial Cr(VI) concentration. When the initial Cr(VI) concentration was 50 mg L^{-1}, the removal efficiency of Cr(VI) reached 89.2% after 60 min of reaction, and when the initial concentration increased to 100, 150, and 200 mg L^{-1}, the corresponding removal efficiencies decreased to 68.9%, 40.7%, and 32.8%, respectively. According to the equations (1) and (2), 1 mol of Fe^0 can theoretically provide 3 mol of electrons for reducing Cr(VI).Therefore, ideally 0.1 g L^{-1} of Cu/Fe bimetallic nanoparticles in an anaerobic environment can fully reduce about 93 mg L^{-1} Cr(VI). However, in this study, the removal amounts of Cr(VI) was 68.92, 61.10 and 65.68 mg L^{-1} at initial Cr(VI) concentrations of 100, 150 and 200 mg L^{-1}, respectively. This may be due to the fact that some of the Fe^0 was oxidized so that the amount of electrons provided by Fe for Cr(VI)

reduction decreased. In addition, we found that the amount of Cr(VI) removal decreased with the initial Cr(VI) concentration (Fig. 7). A possible reason is that with the increase of the initial Cr(VI) concentration, Cr(VI) rapidly occupied the active site on the nZVI surface and formed a Fe(III)-Cr(III) (oxy)hydroxides passivation layer, which inhibited the release of Fe^{2+} and the reduction of Cr(VI) subsequently [43, 47].

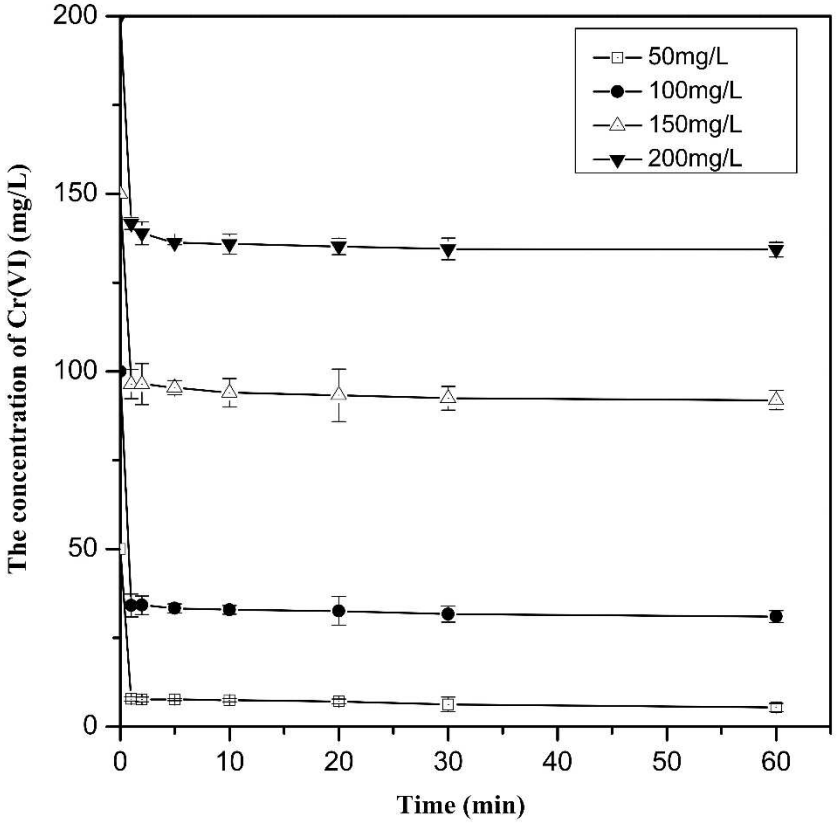

Fig. 7 Effect of initial Cr(VI) concentrations on Cr(VI) removal by Cu/Fe bimetallic nanoparticles. Error bars indicate the standard deviation of the mean (n=3).

The analysis of the Cr(VI) removal process at different initial Cr(VI) concentrations by a pseudo-first-order kinetic model revealed that the k_{obs} decreased as the initial concentration of Cr(VI) increased (Fig. S3, Table 4). When the concentration of Cr(VI) increased from 50 to 100, 150 and 200 mg L^{-1}, the corresponding k_{obs} decreased from 0.0064 to 0.0016, 0.0008 and 0.0006 min^{-1},

respectively. The k_{obs} at low Cr(VI) concentration (50 mg L^{-1}) was almost 10 times higher than that at higher concentrations (200 mg L^{-1}). Similar results were reported by Geng et al [48]. When the initial concentration of Cr(VI) was low, the ratio of nanoparticles/Cr(VI) was relatively high, resulting in a relatively high probability of Cr(VI) contact with Cu/Fe bimetallic nanoparticles, which in turn accelerated the reaction rate.

Table 4. Effect of initial Cr(VI) concentrations on the kinetics of Cr(VI) reduction by Cu/Fe bimetallic nanoparticles

Initial Cr(VI) concentration (mg L^{-1})	k_{obs} (min^{-1})	R^2
50	0.0064	0.9766
100	0.0016	0.8882
150	0.0008	0.7780
200	0.0006	0.4874

3.5 XPS analysis

The products in the reduction of Cr(VI) by the Cu/Fe bimetallic nanoparticles were analyzed by XPS (Fig. 8). The reaction products mainly consisted of Fe, Cr, O and C elements. The photoelectron peak for Cr at about 577 eV indicated that Cr could become a solid-phase deposit attached to the surface of Cu/Fe nanoparticles after the reaction [49]. The main way for Cr(VI) removal is the redox reaction of nZVI with Cr(VI), which produce Fe(III) and Cr(□). This process consumes H^+, thus Fe(III) and Cr(III) can combine with OH^- to form $Fe(OH)_3$, $Cr(OH)_3$, or $Cr_xFe_{1-x}(OH)_3$ coprecipitation [50]. Since the Cu/Fe nanoparticle is a bimetal system, when the insoluble film forms on the surface of the iron particle, the electrons of nZVI can still transfers through the Cu layer to Cr(VI) [26]. Therefore, the reaction can continue as long as the Cu layer is not completely covered by the oxide film.

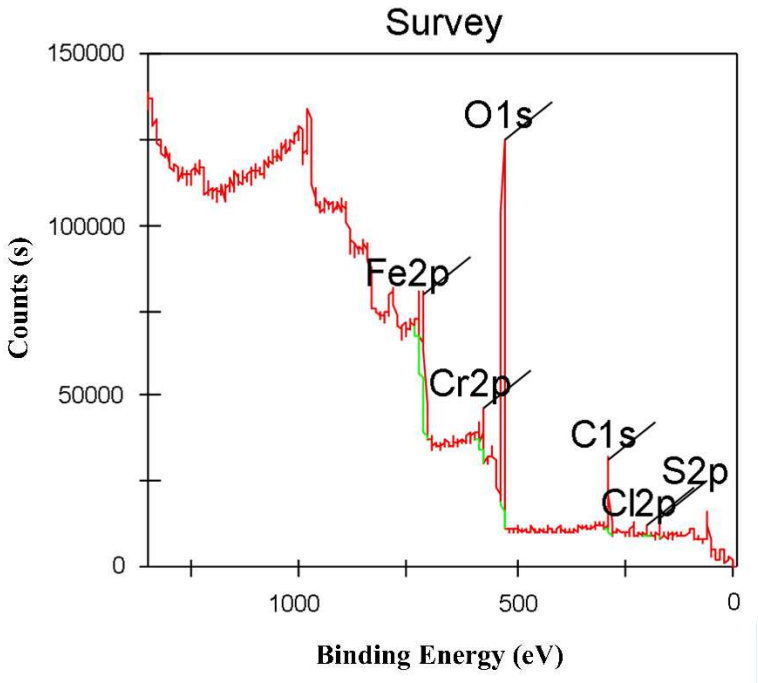

Fig. 8 XPS wide survey of Cu/Fe bimetallic nanoparticles after removal reaction with Cr(VI)

To further analyze the chemical compositions of Cr and Fe, detailed XPS spectra for Cr 2p and Fe 2p were carried out (Fig. 9 and Fig. 10). The Cr $2p_{3/2}$ and Cr $2p_{1/2}$ photoelectron peaks at 577.0 eV and 586.8 eV represent the binding energies of $Cr(OH)_3$, Cr(OH)O, and Cr_2O_3. [40, 51, 52]. The spin-orbit splitting energy is 9.8 eV and Full-Width at Half-Maximum (FWHM) is 3.0 eV, indicating that Cr(III) is the dominant species of Cr on the particle surface [53, 54]. The photoelectron peak for Cr(VI) was not detected in the reaction products. This proved that Cr(VI) was reduced to Cr(III) by interaction with Cu/Fe bimetallic nanoparticles and was eventually deposited on the particle surface. The Fe $2p_{3/2}$ and Fe $2p_{1/2}$ photoelectron peaks at 711.3 eV and 725.2 eV indicate the Fe(III) species in the product, with possible chemical structures of hydrated ferric oxide (FeOOH), magnetite (Fe_3O_4) or hematite (Fe_2O_3) [40]. Besides, there was a satellite peak between two dominant peaks, which indicated a shake-up process of Fe^{2+} [25]. In the study reported by Li et al. [55], a photoelectron peak at 706.9 eV was observed after nZVI was exposed to Cr(VI) solution, which meant the existence of Fe^0 on the surface of reaction products. In our study, few peak of Fe^0

was detected in the Fe 2p spectra, indicating that the Fe^0 in the Cu/Fe nanoparticles had been oxidized to Fe(□) after the reaction. Compared with the case studied by Li et al. [55], it can be demonstrated that the reaction of nZVI with Cr(VI) generates oxide film on the surface, which affects the efficiency of Cr(VI) removal, while the loading of Cu can reduce the passivation of nZVI and make the reaction of nZVI with Cr(VI) more complete.

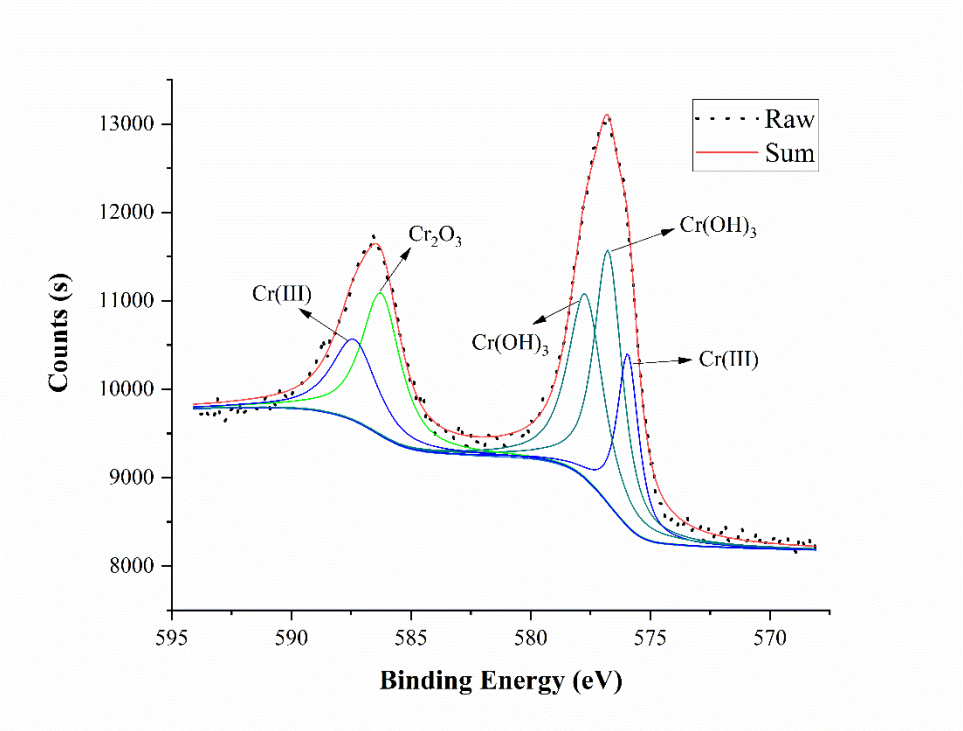

Fig. 9 Cr2p XPS spectra of Cu/Fe bimetallic nanoparticles after removal reaction with Cr(VI)

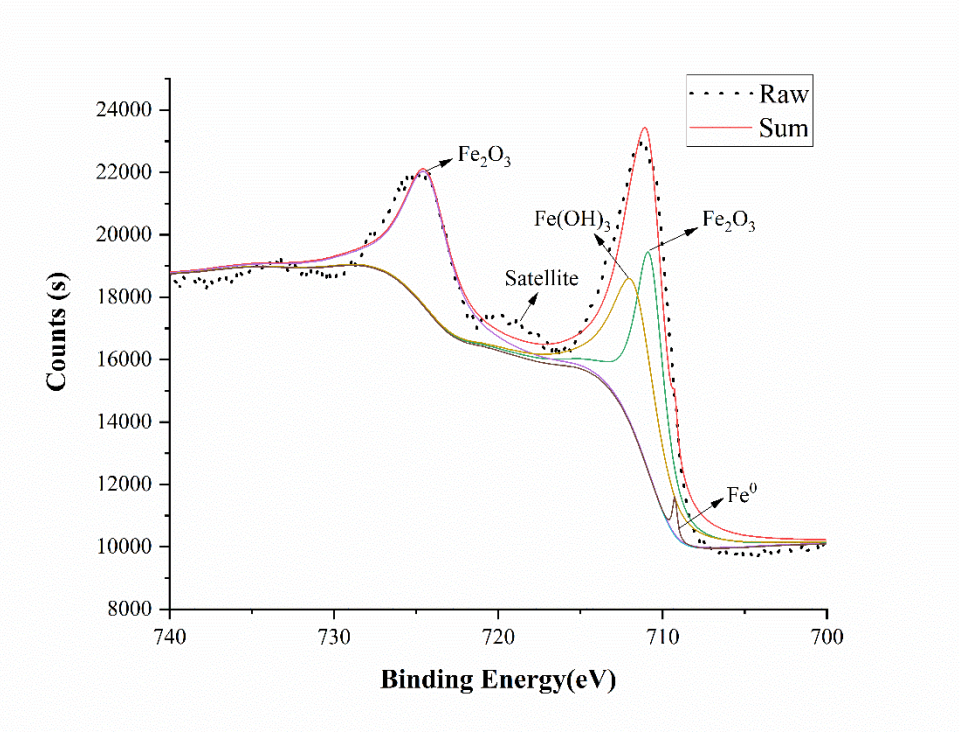

Fig. 10 Fe2p XPS spectra of Cu/Fe bimetallic nanoparticles after removal reaction with Cr(VI)

4. Conclusion

In this study, it was found that the loading of Cu can significantly increase the specific surface area of nZVI, while the degree of oxidation of Fe^0 can be attenuated. The Cu/Fe bimetallic nanoparticles can effectively remove Cr(VI) from the solution, with the best removal capability at the Cu loading rate of 3%. The initial pH and Cr(VI) concentration of the wastewater also affected the removal of Cr(VI) by Cu/Fe bimetallic nanoparticles, and the removal efficiency decreases with increasing pH and Cr(VI) concentration. After the reaction, the Cr(VI) in solution was reduced to Cr(□) and precipitated on the surface of the particles, while Fe^0 was precipitated as an oxide of Fe(□). The results of this study could provide a theoretical basis for the application of iron-based nanomaterials in remediation of wastewater.

Ethics approval and consent to participate

Not applicable.

Consent for publication

Not applicable.

Availability of data and materials

Some of the data have yet to be published, so data will not be shared.

Competing interests

We have no competing interests.

Funding

This study is supported by the National Key Research and Development Program of China (2018YFC1802203) and the National Natural Science Foundation of China (41721001).

Author Contributions

Conceptualization, J.Y., Y.W. and J.S.; methodology, Y.W.; validation, Q.X., H.W. and J.T.; investigation, J.Y., Q.X.; data curation, J.Y and Y.W.; writing—original draft preparation, J.Y.; writing—review and editing, Y.W and J.S.; project administration, J.S.; funding acquisition, J.S. All authors have read and agreed to the published version of the manuscript.

Acknowledgements

Not applicable.

References:

[1] D.M. Hausladen, A. Alexander-Ozinskas, C. McClain, S. Fendorf, Hexavalent chromium sources and distribution in California groundwater, Environmental Science & Technology, 52 (2018) 8242-8251.doi:10.1021/acs.est.7b06627

[2] T. Scarazzato, Z. Panossian, J.A.S. Tenorio, V. Perez-Herranz, D.C.R. Espinosa, A review of cleaner production in electroplating industries using electrodialysis, Journal of Cleaner Production, 168 (2017) 1590-1602.doi:10.1016/j.jclepro.2017.03.152

[3] J. Johnson, L. Schewel, T.E. Graedel, The contemporary anthropogenic chromium cycle, Environmental Science & Technology, 40 (2006) 7060-7069.doi:10.1021/es060061i

[4] R.J. Bartlett, Chromium cycling in soils and water - links, gaps, and methods, Environmental Health Perspectives, 92 (1991) 17-24.doi:10.1289/ehp.919217

[5] D.M. Proctor, M. Suh, L. Mittal, S. Hirsch, R.V. Salgado, C. Bartlett, C. Van Landingham, A. Rohr,

K. Crump, Inhalation cancer risk assessment of hexavalent chromium based on updated mortality for Painesville chromate production workers, Journal of Exposure Science and Environmental Epidemiology, 26 (2016) 224-231.doi:10.1038/jes.2015.77
[6] C.E. Barrera-Diaz, V. Lugo-Lugo, B. Bilyeu, A review of chemical, electrochemical and biological methods for aqueous Cr(VI) reduction, Journal of Hazardous Materials, 223 (2012) 1-12.doi:10.1016/j.jhazmat.2012.04.054
[7] Y. Luo, B. Ye, J. Ye, J. Pang, Q. Xu, J. Shi, B. Long, J. Shi, Ca2+ and SO42- accelerate the reduction of Cr(VI) by Penicilliurn oxalicum SL2, Journal of Hazardous Materials, 382 (2020).doi:10.1016/j.jhazmat.2019.121072
[8] B. Long, J. Ye, Z. Ye, J. He, Y. Luo, Y. Zhao, J. Shi, Cr(VI) removal by Penicillium oxalicum SL2: Reduction with acidic metabolites and form transformation in the mycelium, Chemosphere, 253 (2020).doi:10.1016/j.chemosphere.2020.126731
[9] R.A. Crane, T.B. Scott, Nanoscale zero-valent iron: Future prospects for an emerging water treatment technology, Journal of Hazardous Materials, 211 (2012) 112-125.doi:10.1016/j.jhazmat.2011.11.073
[10] F. Fu, D.D. Dionysiou, H. Liu, The use of zero-valent iron for groundwater remediation and wastewater treatment: A review, Journal of Hazardous Materials, 267 (2014) 194-205.doi:10.1016/j.jhazmat.2013.12.062
[11] D. O'Carroll, B. Sleep, M. Krol, H. Boparai, C. Kocur, Nanoscale zero valent iron and bimetallic particles for contaminated site remediation, Advances in Water Resources, 51 (2013) 104-122.doi:10.1016/j.advwatres.2012.02.005
[12] J. Scaria, P.V. Nidheesh, M.S. Kumar, Synthesis and applications of various bimetallic nanomaterials in water and wastewater treatment, Journal of Environmental Management, 259 (2020).doi:10.1016/j.jenvman.2019.110011
[13] M. Stefaniuk, P. Oleszczuk, Y.S. Ok, Review on nano zerovalent iron (nZVI): From synthesis to environmental applications, Chemical Engineering Journal, 287 (2016) 618-632.doi:10.1016/j.cej.2015.11.046
[14] H. Dong, J. Deng, Y. Xie, C. Zhang, Z. Jiang, Y. Cheng, K. Hou, G. Zeng, Stabilization of nanoscale zero-valent iron (nZVI) with modified biochar for Cr(VI) removal from aqueous solution, Journal of Hazardous Materials, 332 (2017) 79-86.doi:10.1016/j.jhazmat.2017.03.002
[15] E. Petala, K. Dimos, A. Douvalis, T. Bakas, J. Tucek, R. Zboril, M.A. Karakassides, Nanoscale zero-valent iron supported on mesoporous silica: Characterization and reactivity for Cr(VI) removal from aqueous solution, Journal of Hazardous Materials, 261 (2013) 295-306.doi:10.1016/j.jhazmat.2013.07.046
[16] L. Shi, X. Zhang, Z. Chen, Removal of Chromium (VI) from wastewater using bentonite-supported nanoscale zero-valent iron, Water Research, 45 (2011) 886-892.doi:10.1016/j.watres.2010.09.025
[17] Y. Gong, L. Gai, J. Tang, J. Fu, Q. Wang, E.Y. Zeng, Reduction of Cr(VI) in simulated groundwater by FeS-coated iron magnetic nanoparticles, Science of the Total Environment, 595 (2017) 743-751.doi:10.1016/j.scitotenv.2017.03.282
[18] X. Wang, M. Zhu, H. Liu, J. Ma, F. Li, Modification of Pd-Fe nanoparticles for catalytic dechlorination of 2,4-dichlorophenol, Science of the Total Environment, 449 (2013) 157-167.doi:10.1016/j.scitotenv.2013.01.008
[19] D. Jiang, D. Huang, C. Lai, P. Xu, G. Zeng, J. Wan, L. Tang, H. Dong, B. Huang, T. Hu, Difunctional chitosan-stabilized Fe/Cu bimetallic nanoparticles for removal of hexavalent chromium wastewater, Science of the Total Environment, 644 (2018) 1181-1189.doi:10.1016/j.scitotenv.2018.06.367

[20] Y. Lv, Z. Niu, Y. Chen, Y. Hu, Bacterial effects and interfacial inactivation mechanism of nZVI/Pd on Pseudomonas putida strain, Water Research, 115 (2017) 297-308.doi:10.1016/j.watres.2017.03.012
[21] Y.H. Kim, E.R. Carraway, Dechlorination of chlorinated ethenes and acetylenes by palladized iron, Environmental Technology, 24 (2003) 809-819.doi:10.1080/09593330309385618
[22] Y. Li, X. Li, D. Han, W. Huang, C. Yang, New insights into the role of Ni loading on the surface structure and the reactivity of nZVI toward tetrabromo- and tetrachlorobisphenol A, Chemical Engineering Journal, 311 (2017) 173-182.doi:10.1016/j.cej.2016.11.084
[23] H. Dong, Z. Jiang, J. Deng, C. Zhang, Y. Cheng, K. Hou, L. Zhang, L. Tang, G. Zeng, Physicochemical transformation of Fe/Ni bimetallic nanoparticles during aging in simulated groundwater and the consequent effect on contaminant removal, Water Research, 129 (2018) 51-57.doi:10.1016/j.watres.2017.11.002
[24] F. Zhu, L. Li, S. Ma, Z. Shang, Effect factors, kinetics and thermodynamics of remediation in the chromium contaminated soils by nanoscale zero valent Fe/Cu bimetallic particles, Chemical Engineering Journal, 302 (2016) 663-669.doi:10.1016/j.cej.2016.05.072
[25] S. Zhou, Y. Li, J. Chen, Z. Liu, Z. Wang, P. Na, Enhanced Cr(VI) removal from aqueous solutions using Ni/Fe bimetallic nanoparticles: characterization, kinetics and mechanism, Rsc Advances, 4 (2014) 50699-50707.doi:10.1039/c4ra08754b
[26] C. Hu, S. Lo, Y. Liou, Y. Hsu, K. Shih, C. Lin, Hexavalent chromium removal from near natural water by copper-iron bimetallic particles, Water Research, 44 (2010) 3101-3108.doi:10.1016/j.watres.2010.02.037
[27] R. Yamaguchi, S. Kurosu, M. Suzuki, Y. Kawase, Hydroxyl radical generation by zero-valent iron/Cu (ZVI/Cu) bimetallic catalyst in wastewater treatment: Heterogeneous Fenton/Fenton-like reactions by Fenton reagents formed in-situ under oxic conditions, Chemical Engineering Journal, 334 (2018) 1537-1549.doi:10.1016/j.cej.2017.10.154
[28] W. Liu, T. Qian, H. Jiang, Bimetallic Fe nanoparticles: Recent advances in synthesis and application in catalytic elimination of environmental pollutants, Chemical Engineering Journal, 236 (2014) 448-463.doi:10.1016/j.cej.2013.10.062
[29] B. Lai, Y. Zhang, Z. Chen, P. Yang, Y. Zhou, J. Wang, Removal of p-nitrophenol (PNP) in aqueous solution by the micron-scale iron-copper (Fe/Cu) bimetallic particles, Applied Catalysis B-Environmental, 144 (2014) 816-830.doi:10.1016/j.apcatb.2013.08.020
[30] S.J. Bransfield, D.M. Cwiertny, A.L. Roberts, D.H. Fairbrother, Influence of copper loading and surface coverage on the reactivity of granular iron toward 1,1,1-trichloroethane, Environmental Science & Technology, 40 (2006) 1485-1490.doi:10.1021/es051300p
[31] C. Wang, W. Zhang, Synthesizing nanoscale iron particles for rapid and complete dechlorination of TCE and PCBs, Environmental Science & Technology, 31 (1997) 2154-2156.doi:10.1021/es970039c
[32] Y. Sun, X. Li, J. Cao, W. Zhang, H.P. Wang, Characterization of zero-valent iron nanoparticles, Advances in Colloid and Interface Science, 120 (2006) 47-56.doi:10.1016/j.cis.2006.03.001
[33] J. Lin, M. Sun, X. Liu, Z. Chen, Functional kaolin supported nanoscale zero-valent iron as a Fenton-like catalyst for the degradation of Direct Black G, Chemosphere, 184 (2017) 664-672.doi:10.1016/j.chemosphere.2017.06.038
[34] X. Zhang, S. Lin, Z. Chen, M. Megharaj, R. Naidu, Kaolinite-supported nanoscale zero-valent iron for removal of Pb2+ from aqueous solution: Reactivity, characterization and mechanism, Water Research, 45 (2011) 3481-3488.doi:10.1016/j.watres.2011.04.010
[35] Y. Yuan, Z. An, L. Zhang, Y. Zhang, B. Shi, Z. Xiong, B. Lai, The influence of Cu(II) existence state

on characteristics, reactivity, and recyclability of microscale Fe/Cu bimetal, Industrial & Engineering Chemistry Research, 59 (2020) 7310-7320.doi:10.1021/acs.iecr.0c00243
[36] T.Y. Liu, Z.L. Wang, L. Zhao, X. Yang, Enhanced chitosan/Fe-0-nanoparticles beads for hexavalent chromium removal from wastewater, Chemical Engineering Journal, 189 (2012) 196-202.doi:10.1016/j.cej.2012.02.056
[37] H. Qian, Y. Wu, Y. Liu, X. Xu, Kinetics of hexavalent chromium reduction by iron metal, Frontiers of Environmental Science and Engineering in China, 2 (2008) 51-56.doi:10.1007/s11783-008-0010-3
[38] M. Gheju, Hexavalent chromium reduction with zero-valent iron (ZVI) in aquatic systems, Water Air and Soil Pollution, 222 (2011) 103-148.doi:10.1007/s11270-011-0812-y
[39] M. Vitkova, M. Puschenreiter, M. Komarek, Effect of nano zero-valent iron application on As, Cd, Pb, and Zn availability in the rhizosphere of metal(loid) contaminated soils, Chemosphere, 200 (2018) 217-226.doi:10.1016/j.chemosphere.2018.02.118
[40] S. Li, T. You, Y. Guo, S. Yao, S. Zang, M. Xiao, Z. Zhang, Y. Shen, High dispersions of nano zero valent iron supported on biochar by one-step carbothermal synthesis and its application in chromate removal, Rsc Advances, 9 (2019) 12428-12435.doi:10.1039/c9ra00304e
[41] Y.H. Shih, C.Y. Hsu, Y.F. Su, Reduction of hexachlorobenzene by nanoscale zero-valent iron: Kinetics, pH effect, and degradation mechanism, Separation and Purification Technology, 76 (2011) 268-274.doi:10.1016/j.seppur.2010.10.015
[42] S. Mortazavian, H. An, D. Chun, J. Moon, Activated carbon impregnated by zero-valent iron nanoparticles (AC/nZVI) optimized for simultaneous adsorption and reduction of aqueous hexavalent chromium: Material characterizations and kinetic studies, Chemical Engineering Journal, 353 (2018) 781-795.doi:10.1016/j.cej.2018.07.170
[43] D. Lv, J. Zhou, Z. Cao, J. Xu, Y. Liu, Y. Li, K. Yang, Z. Lou, L. Lou, X. Xu, Mechanism and influence factors of chromium(VI) removal by sulfide-modified nanoscale zerovalent iron, Chemosphere, 224 (2019) 306-315.doi:10.1016/j.chemosphere.2019.02.109
[44] Z. Wang, R.T. Bush, L.A. Sullivan, J. Liu, Simultaneous redox conversion of chromium(VI) and arsenic(III) under acidic conditions, Environmental Science & Technology, 47 (2013) 6486-6492.doi:10.1021/es400547p
[45] L. Zhou, A. Li, F. Ma, H.P. Zhao, F.X. Deng, S.S. Pi, A.Q. Tang, J.X. Yang, Combining high electron transfer efficiency and oxidation resistance in nZVI with coatings of microbial extracellular polymeric substances to enhance Sb (V) reduction and adsorption, Chemical Engineering Journal, 395 (2020).doi:10.1016/j.cej.2020.125168
[46] J. Li, M.J. Fana, M. Li, X. Liu, Cr(VI) removal from groundwater using double surfactant-modified nanoscale zero-valent iron (nZVI): Effects of materials in different status, Science of the Total Environment, 717 (2020).doi:10.1016/j.scitotenv.2020.137112
[47] N. Melitas, O. Chuffe-Moscoso, J. Farrell, Kinetics of soluble chromium removal from contaminated water by zerovalent iron media: Corrosion inhibition and passive oxide effects, Environmental Science & Technology, 35 (2001) 3948-3953.doi:10.1021/es001923x
[48] B. Geng, Z. Jin, T. Li, X. Qi, Kinetics of hexavalent chromium removal from water by chitosan-Fe-0 nanoparticles, Chemosphere, 75 (2009) 825-830.doi:10.1016/j.chemosphere.2009.01.009
[49] T. Jia, B. Zhang, L. Huang, S. Wang, C. Xu, Enhanced sequestration of Cr(VI) by copper doped sulfidated zerovalent iron (SZVI-Cu): Characterization, performance, and mechanisms, Chemical Engineering Journal, 366 (2019) 200-207.doi:10.1016/j.cej.2019.02.058
[50] S.C. Liu, H.J. Gao, R. Cheng, Y.J. Wang, X.L. Ma, C. Peng, Z.L. Xie, Study on influencing factors

and mechanism of removal of Cr(VI) from soil suspended liquid by bentonite-supported nanoscale zero-valent iron, Scientific Reports, 10 (2020).doi:10.1038/s41598-020-65814-3
[51] N. Fiol, C. Escudero, I. Villaescusa, Chromium sorption and Cr(VI) reduction to Cr(III) by grape stalks and yohimbe bark, Bioresource Technology, 99 (2008) 5030-5036.doi:10.1016/j.biortech.2007.09.007
[52] Y. Fang, J. Wen, H.B. Zhang, Q. Wang, X.H. Hu, Enhancing Cr(VI) reduction and immobilization by magnetic core-shell structured NZVI@MOF derivative hybrids, Environmental Pollution, 260 (2020).doi:10.1016/j.envpol.2020.114021
[53] B. Geng, Z. Jin, T. Li, X. Qi, Preparation of chitosan-stabilized Fe-0 nanoparticles for removal of hexavalent chromium in water, Science of the Total Environment, 407 (2009) 4994-5000.doi:10.1016/j.scitotenv.2009.05.051
[54] Y. Wang, L. Yu, R.T. Wang, Y. Wang, X.D. Zhang, A novel cellulose hydrogel coating with nanoscale Fe0 for Cr(VI) adsorption and reduction, Science of the Total Environment, 726 (2020).doi:10.1016/j.scitotenv.2020.138625
[55] X. Li, J. Cao, W. Zhang, Stoichiometry of Cr(VI) immobilization using nanoscale zerovalent iron (nZVI): A study with high-resolution X-ray photoelectron Spectroscopy (HR-XPS), Industrial & Engineering Chemistry Research, 47 (2008) 2131-2139.doi:10.1021/ie061655x

Figures

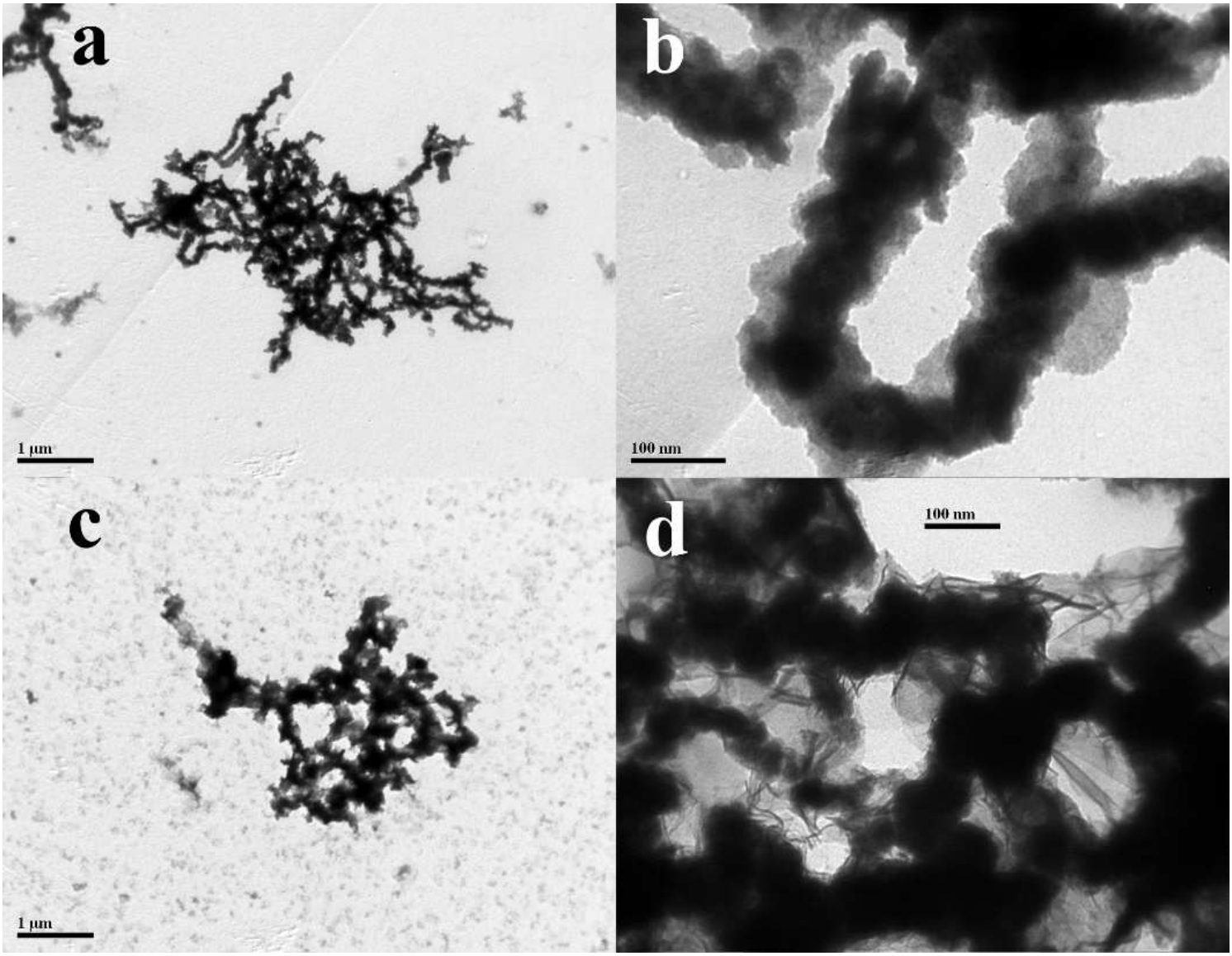

Figure 1

TEM images of nZVI (a, b) and Cu/Fe bimetallic nanoparticles (c, d).

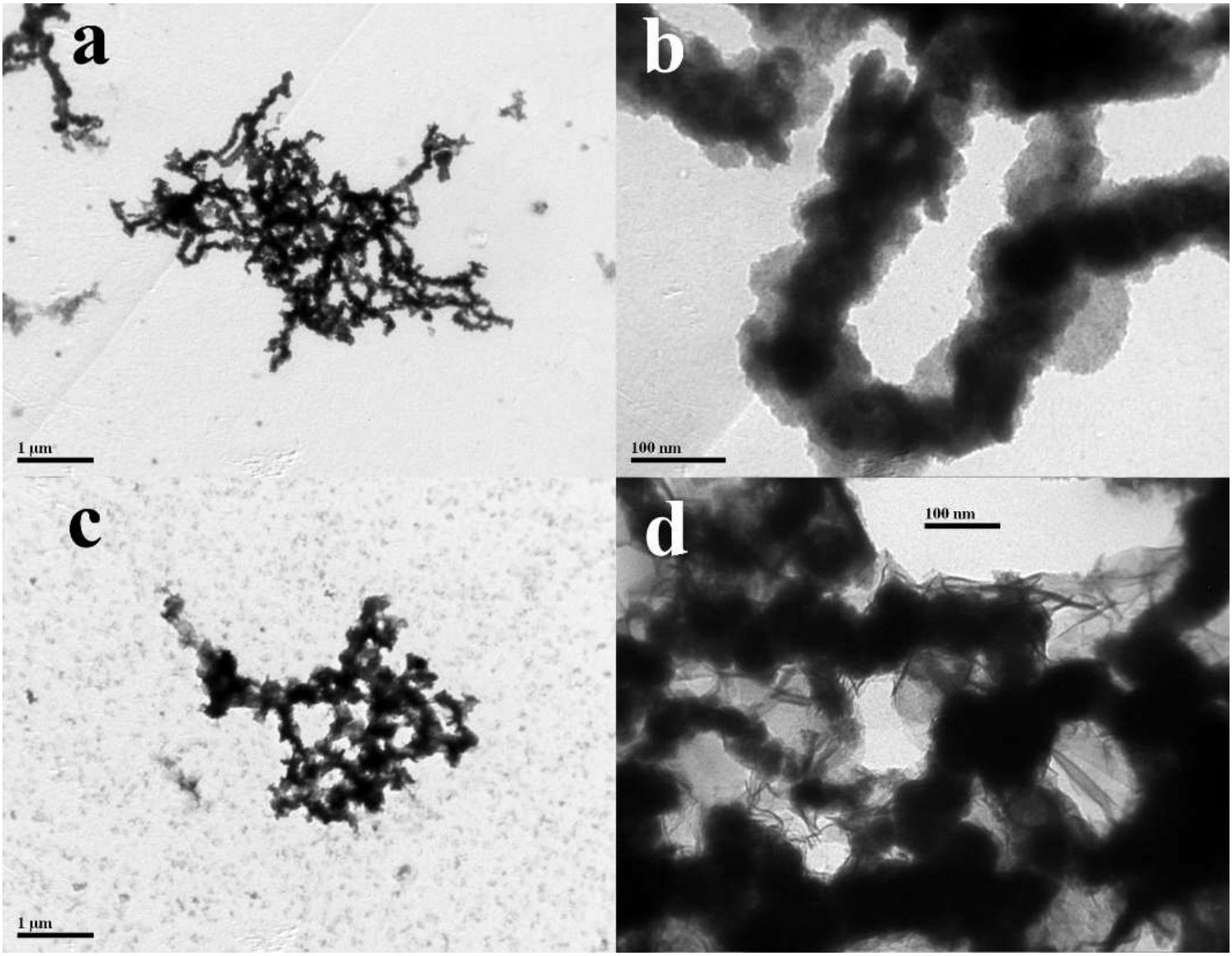

Figure 1

TEM images of nZVI (a, b) and Cu/Fe bimetallic nanoparticles (c, d).

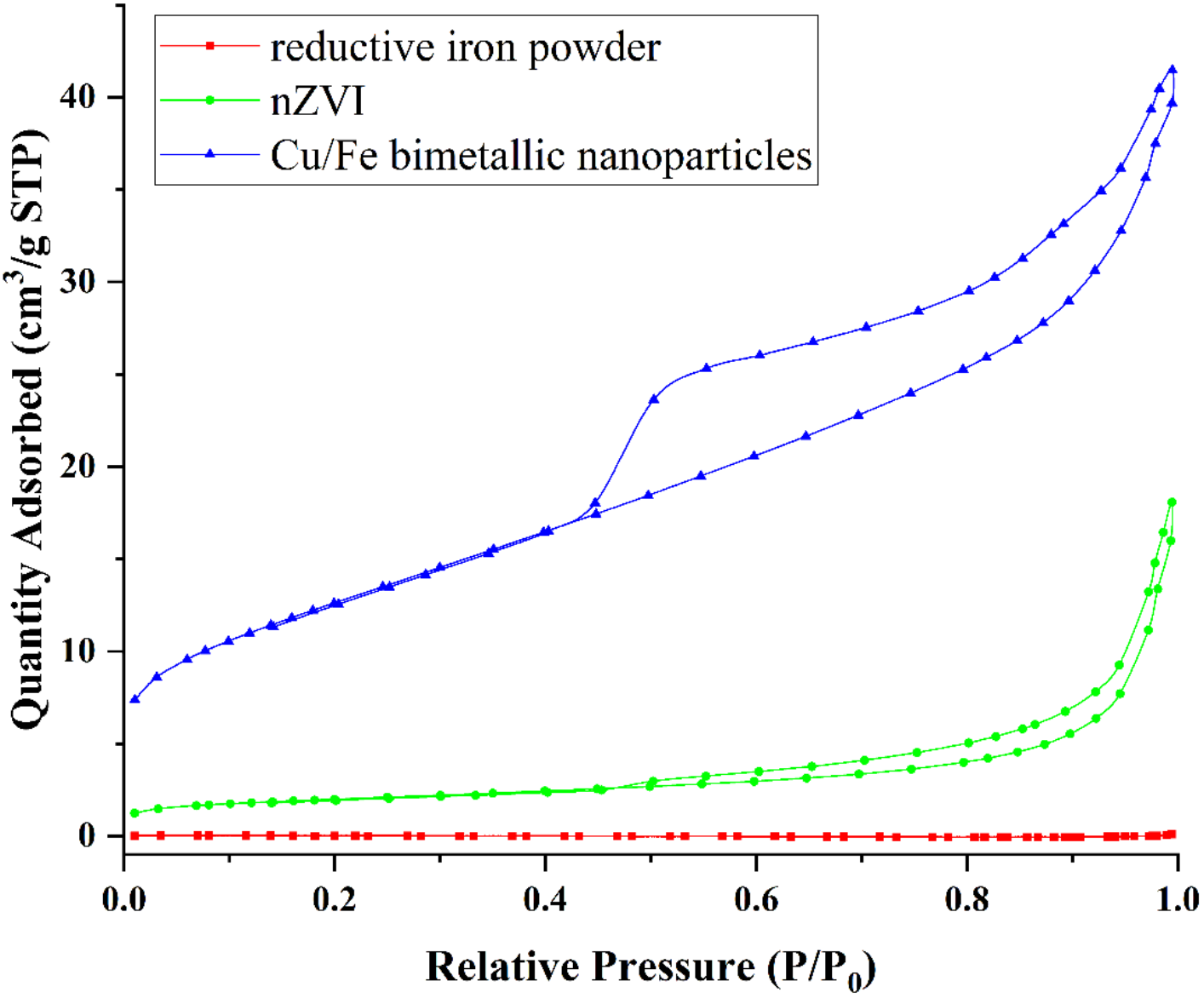

Figure 2

The adsorption-desorption isotherms of reductive iron powder, nZVI, and Cu/Fe bimetallic nanoparticles.

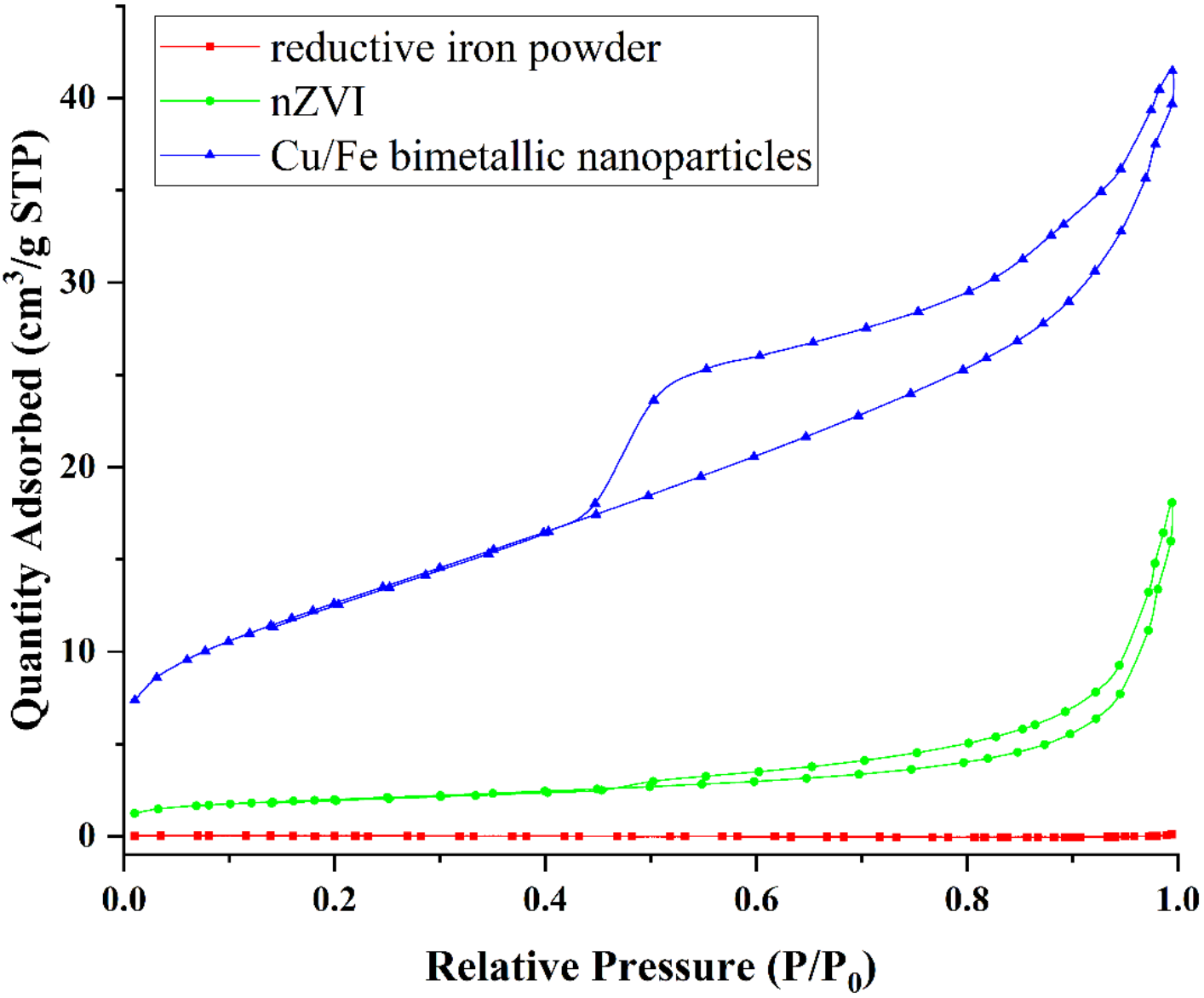

Figure 2

The adsorption-desorption isotherms of reductive iron powder, nZVI, and Cu/Fe bimetallic nanoparticles.

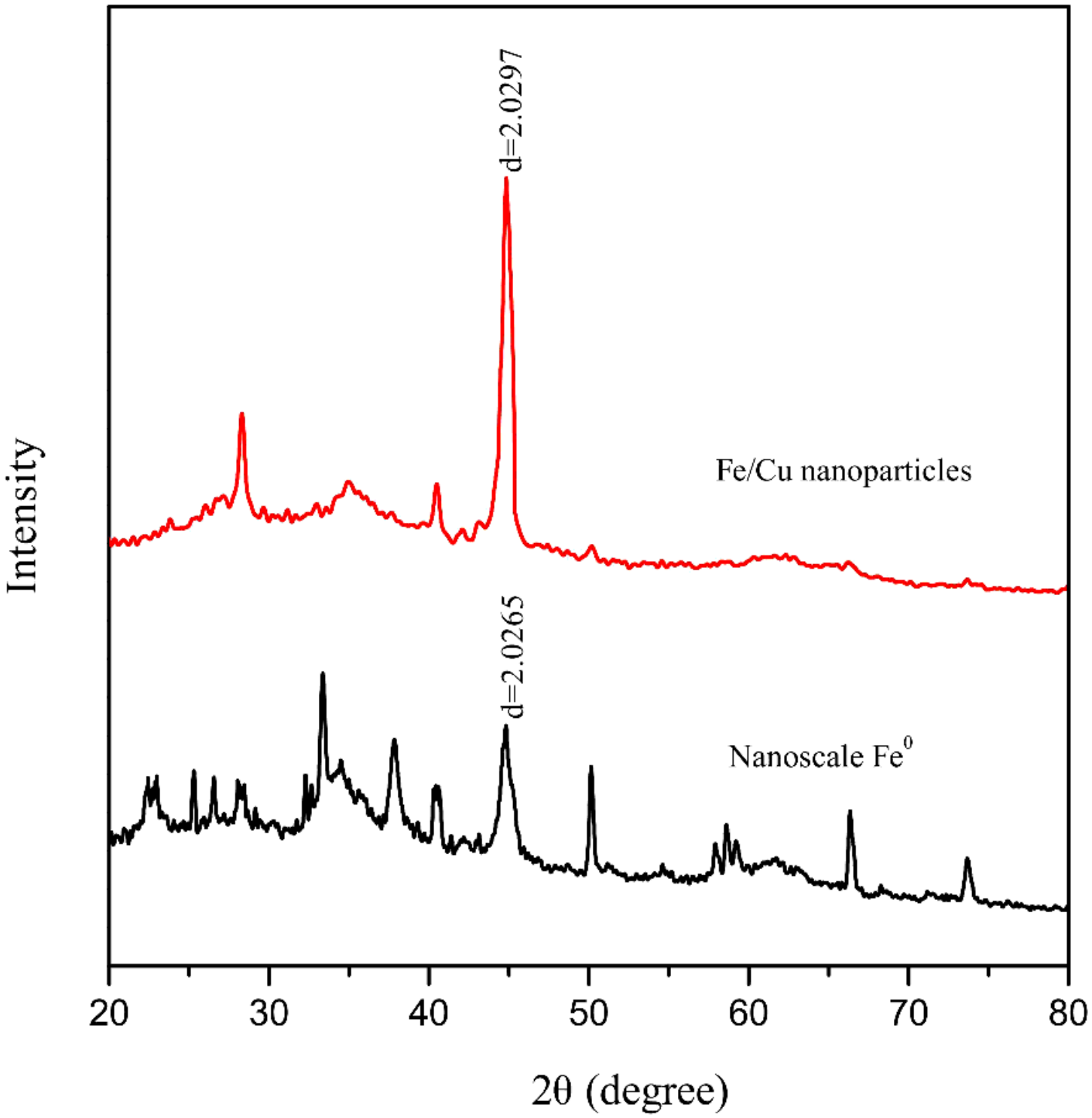

Figure 3

XRD patterns of nZVI and Cu/Fe bimetallic nanoparticles.

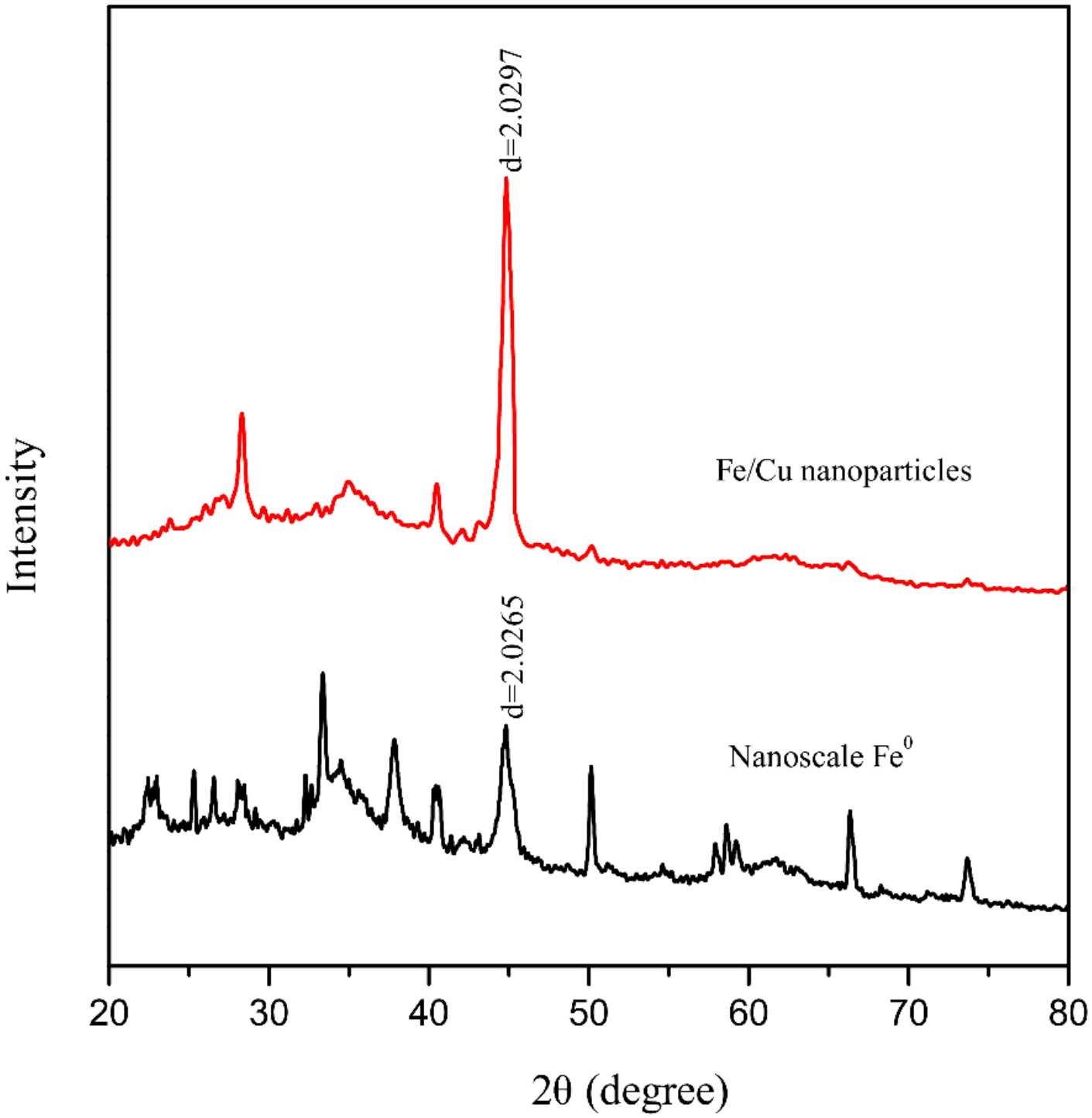

Figure 3

XRD patterns of nZVI and Cu/Fe bimetallic nanoparticles.

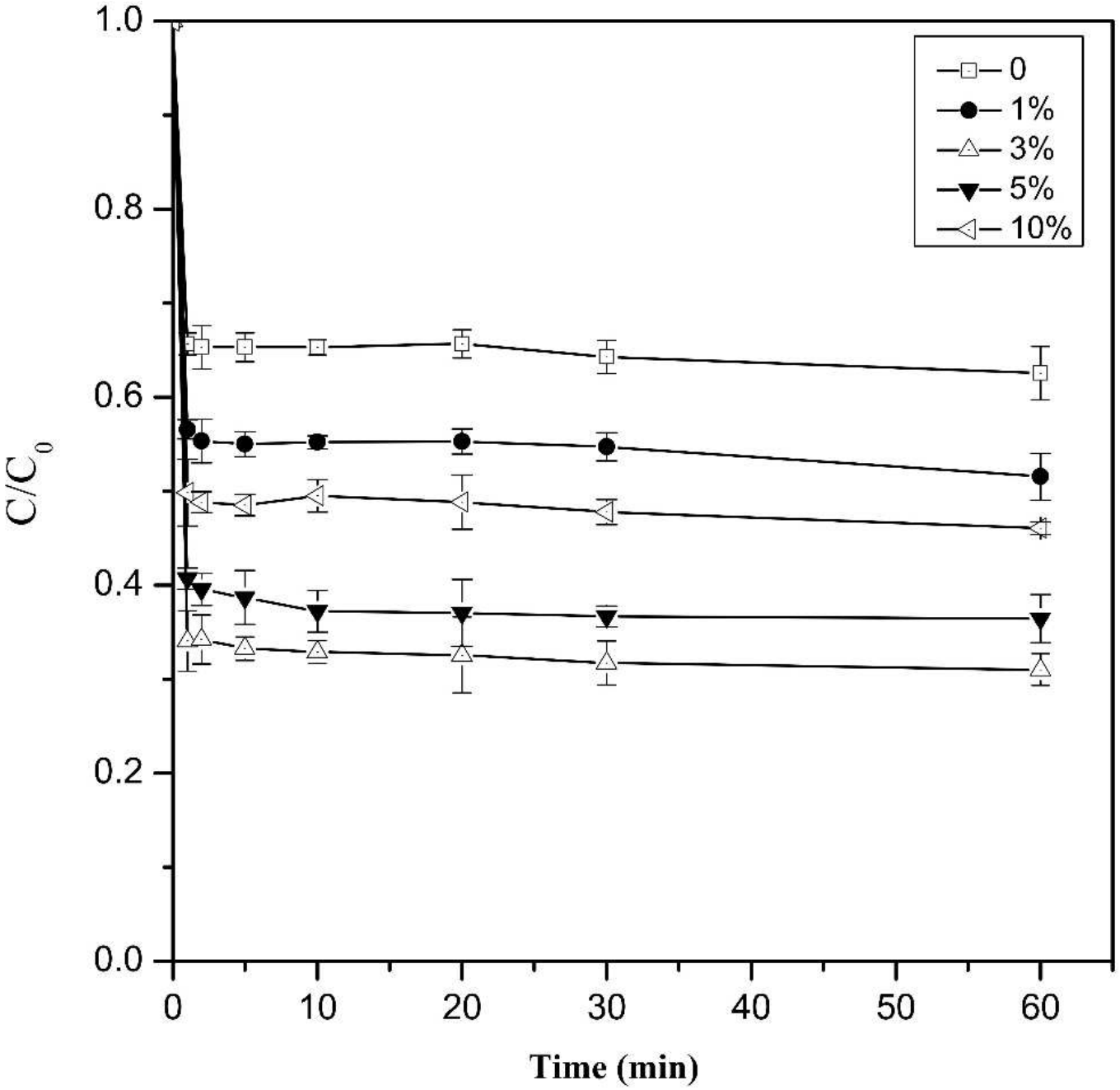

Figure 4

Effect of copper loading rates on Cr(VI) removal by Cu/Fe bimetallic nanoparticles. Error bars indicate the standard deviation of the mean (n=3).

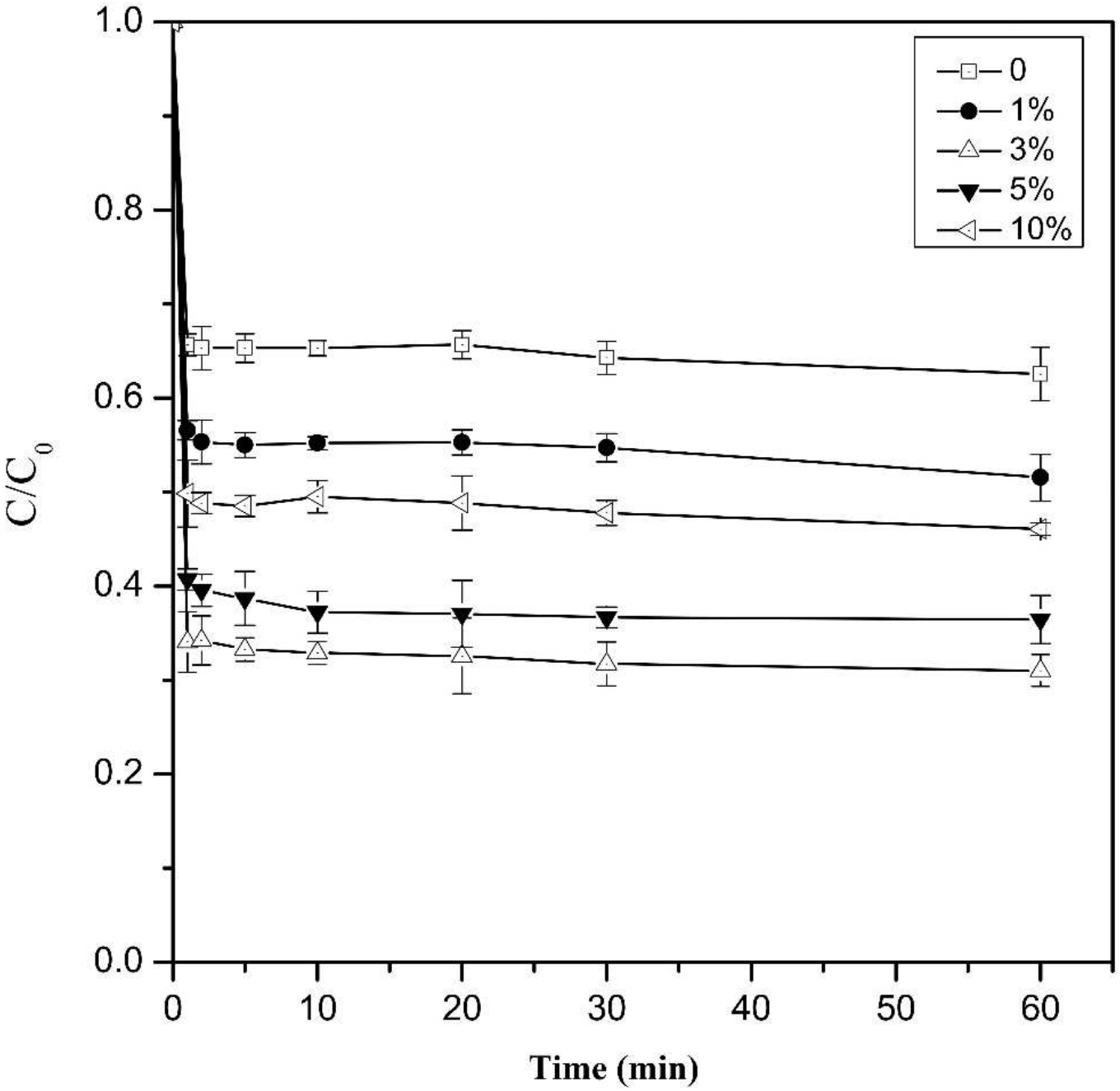

Figure 4

Effect of copper loading rates on Cr(VI) removal by Cu/Fe bimetallic nanoparticles. Error bars indicate the standard deviation of the mean (n=3).

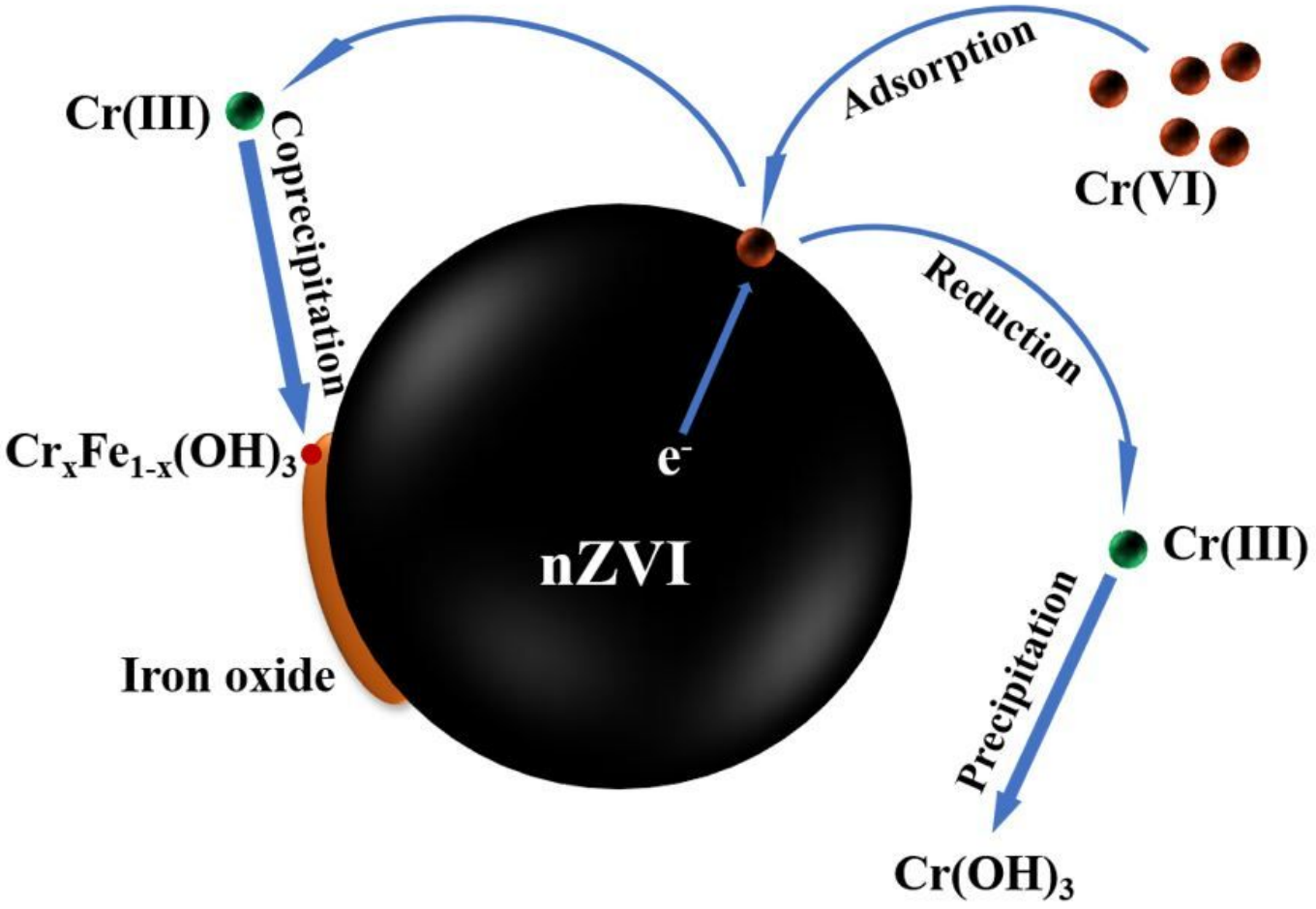

Figure 5

Proposed mechanism for the removal of Cr(VI) using nZVI.

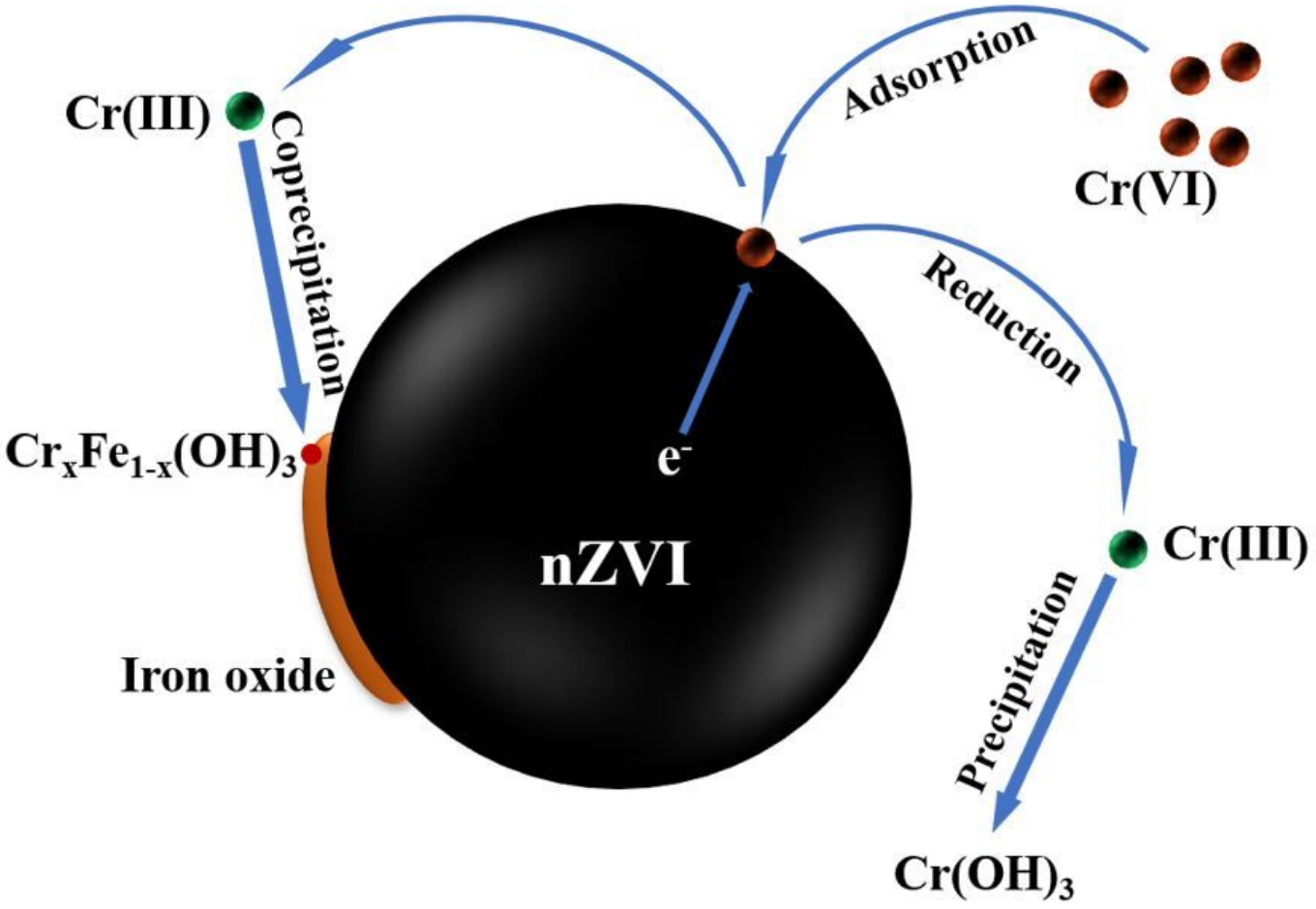

Figure 5

Proposed mechanism for the removal of Cr(VI) using nZVI.

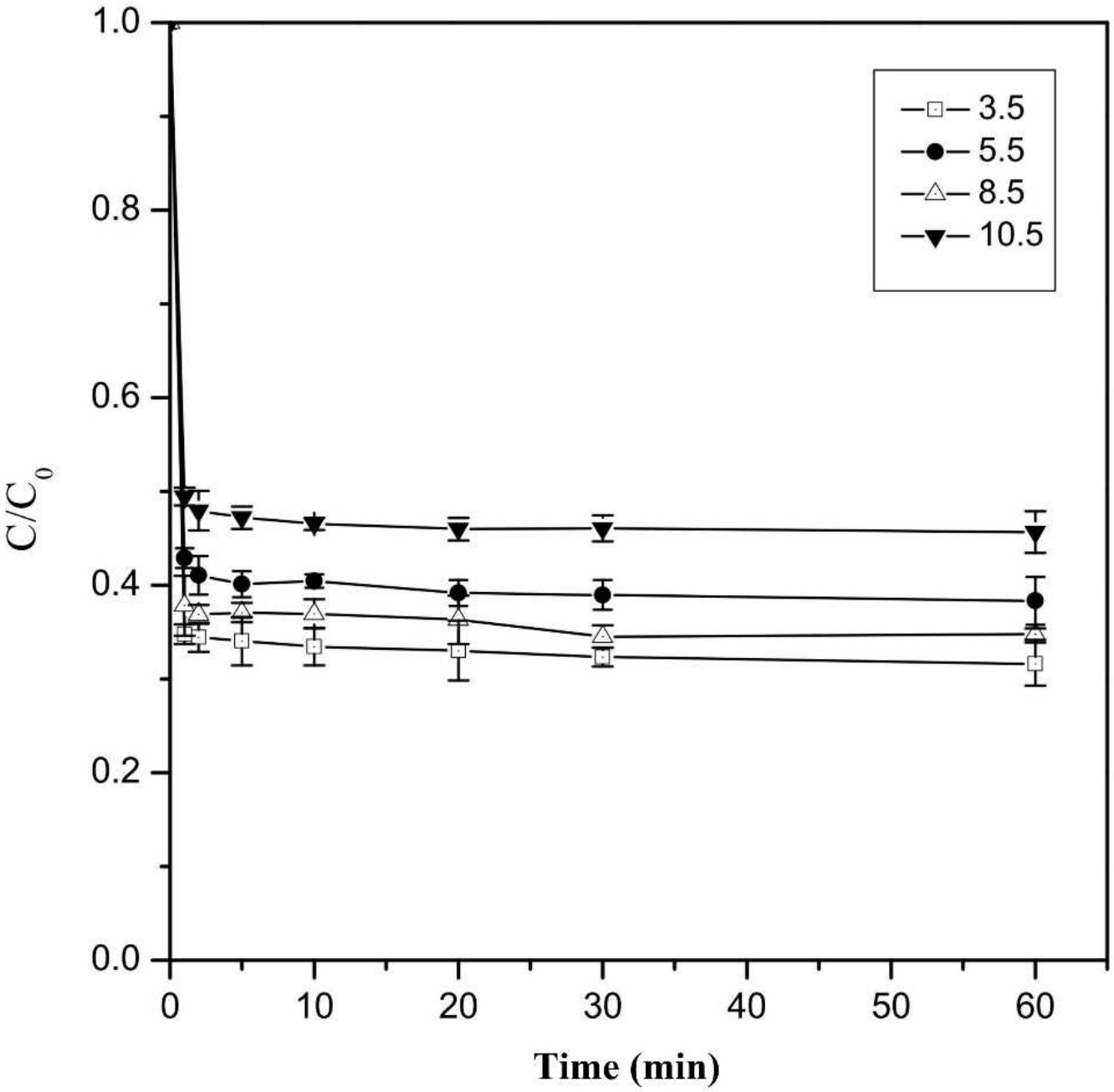

Figure 6

Effect of initial pH on Cr(VI) removal by Cu/Fe bimetallic nanoparticles. Error bars indicate the standard deviation of the mean (n=3).

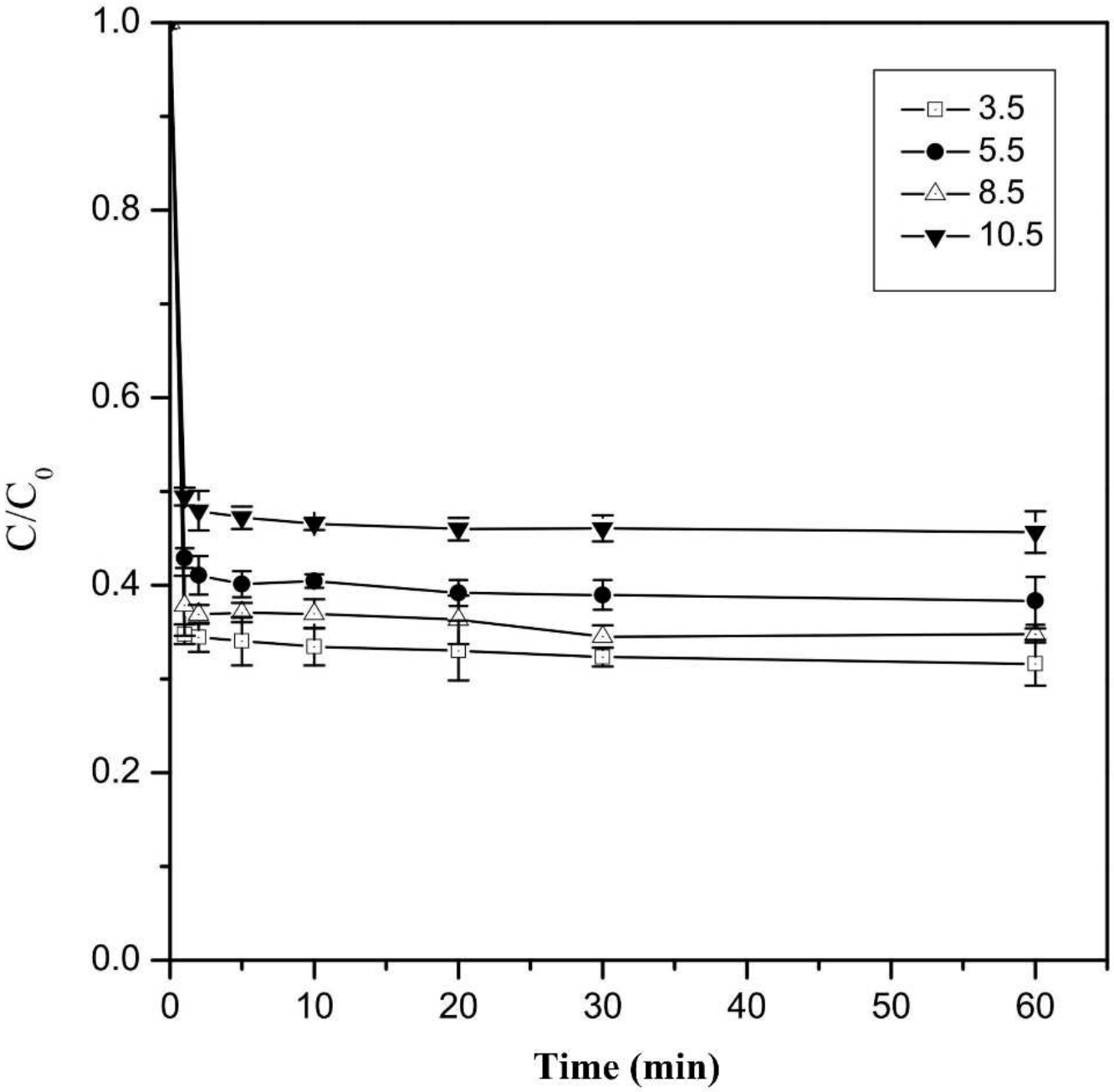

Figure 6

Effect of initial pH on Cr(VI) removal by Cu/Fe bimetallic nanoparticles. Error bars indicate the standard deviation of the mean (n=3).

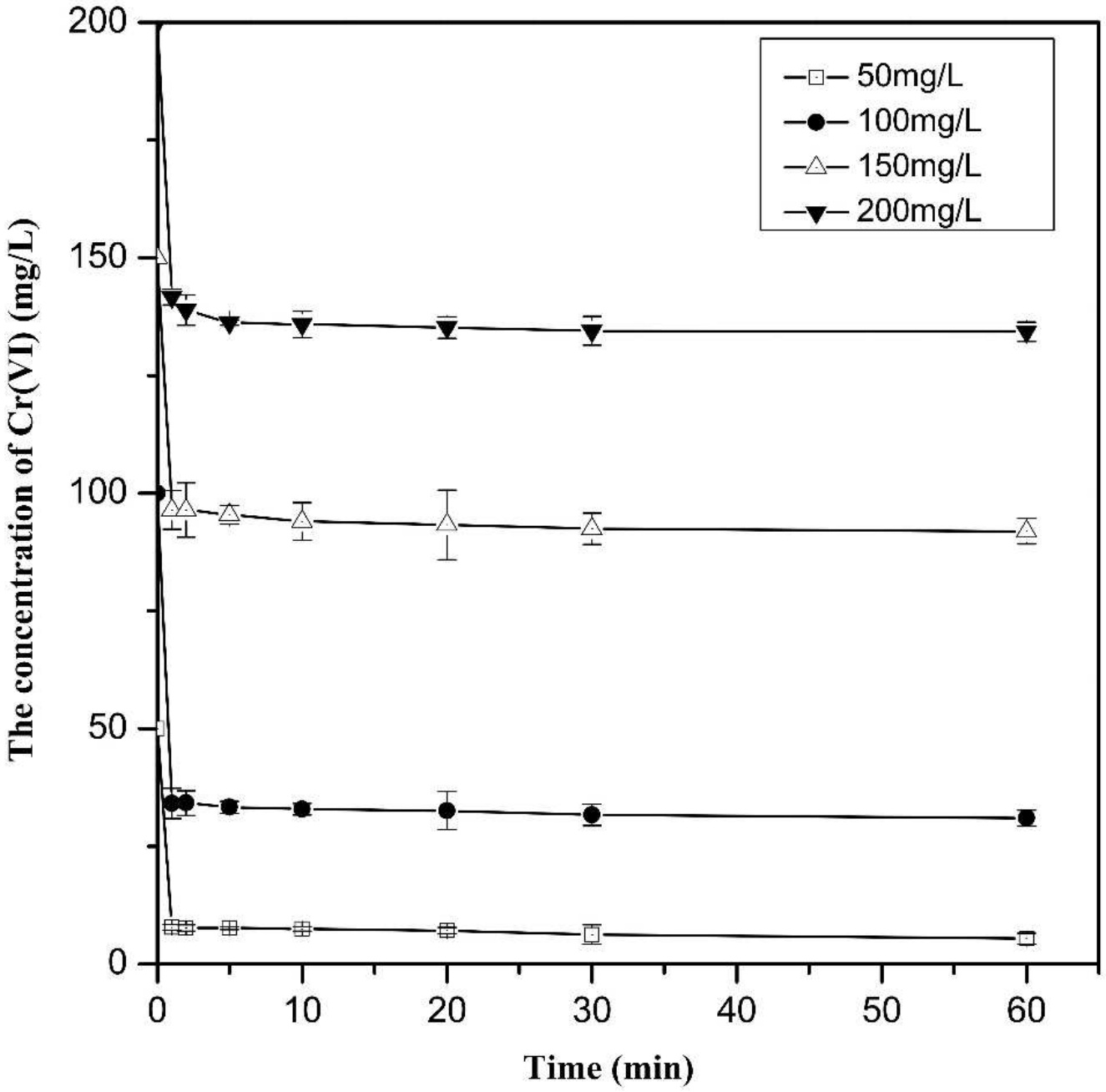

Figure 7

Effect of initial Cr(VI) concentrations on Cr(VI) removal by Cu/Fe bimetallic nanoparticles. Error bars indicate the standard deviation of the mean (n=3).

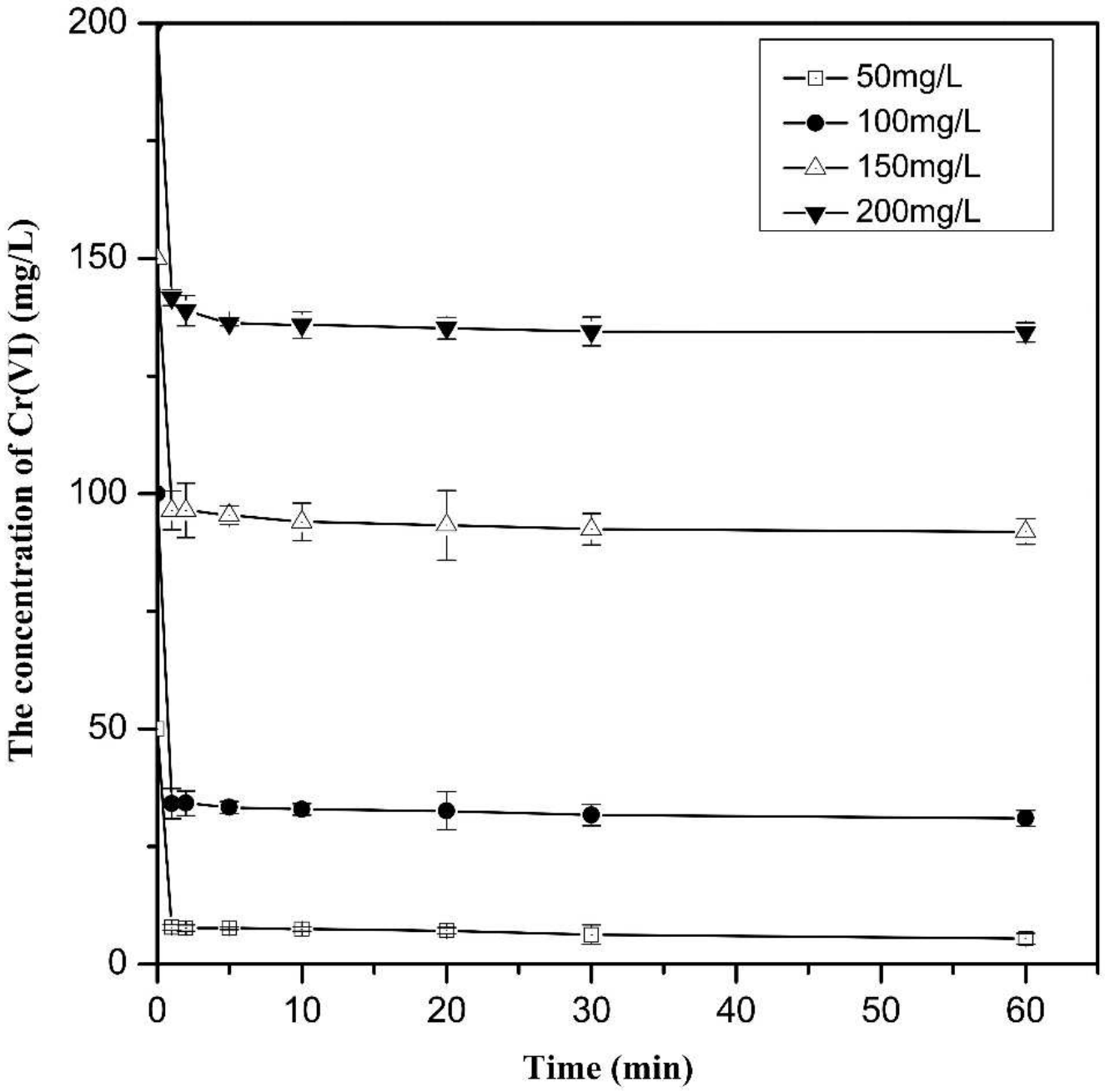

Figure 7

Effect of initial Cr(VI) concentrations on Cr(VI) removal by Cu/Fe bimetallic nanoparticles. Error bars indicate the standard deviation of the mean (n=3).

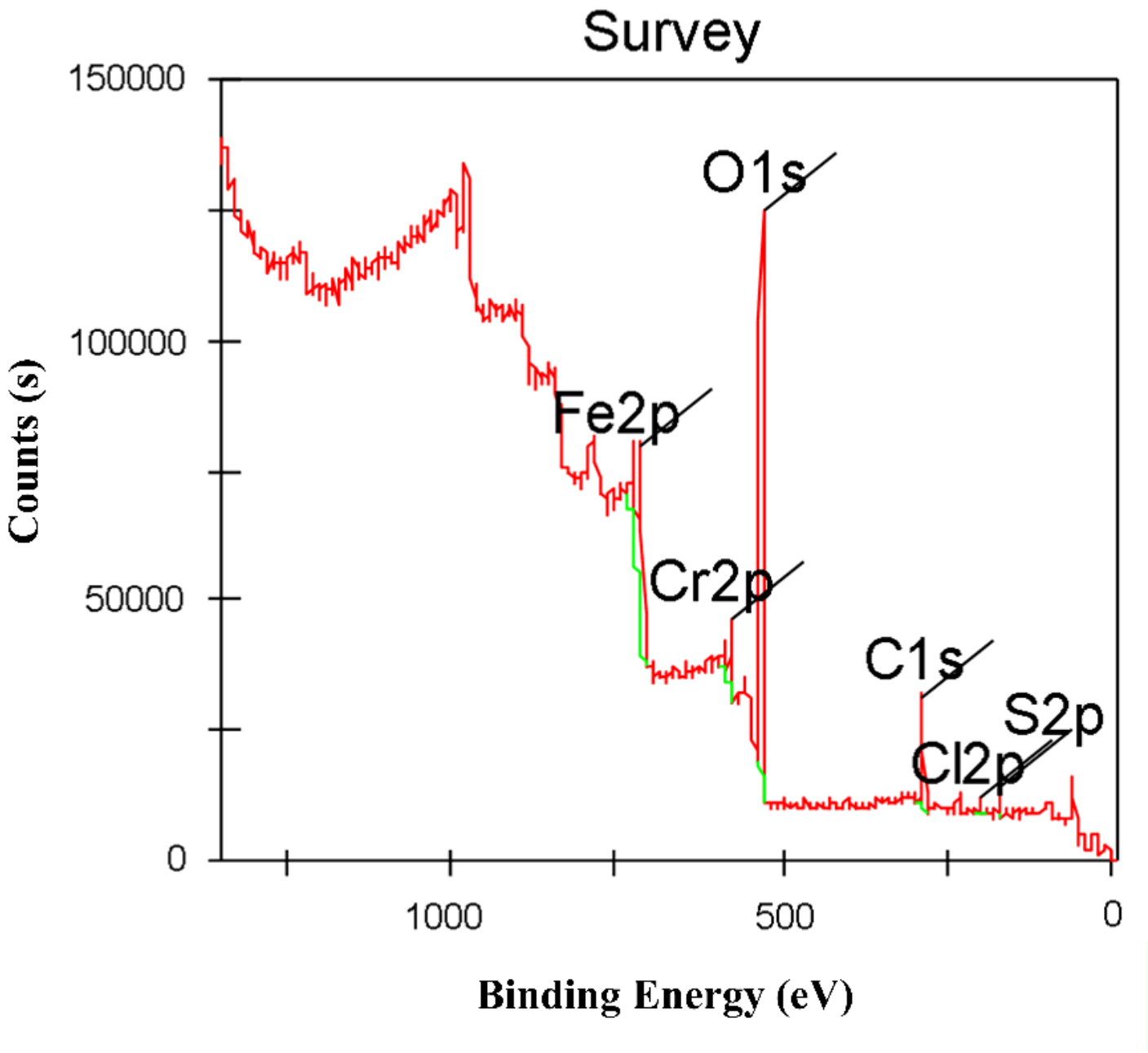

Figure 8

XPS wide survey of Cu/Fe bimetallic nanoparticles after removal reaction with Cr(VI) To further analyze the chemical compositions of Cr and Fe, detailed XPS spectra for Cr 2p and Fe 2p were carried out (Fig. 9 and Fig. 10). The Cr 2p3/2 and Cr 2p1/2 photoelectron peaks at 577.0 eV and 586.8 eV represent the binding energies of Cr(OH)3, Cr(OH)O, and Cr2O3. [40, 51, 52].

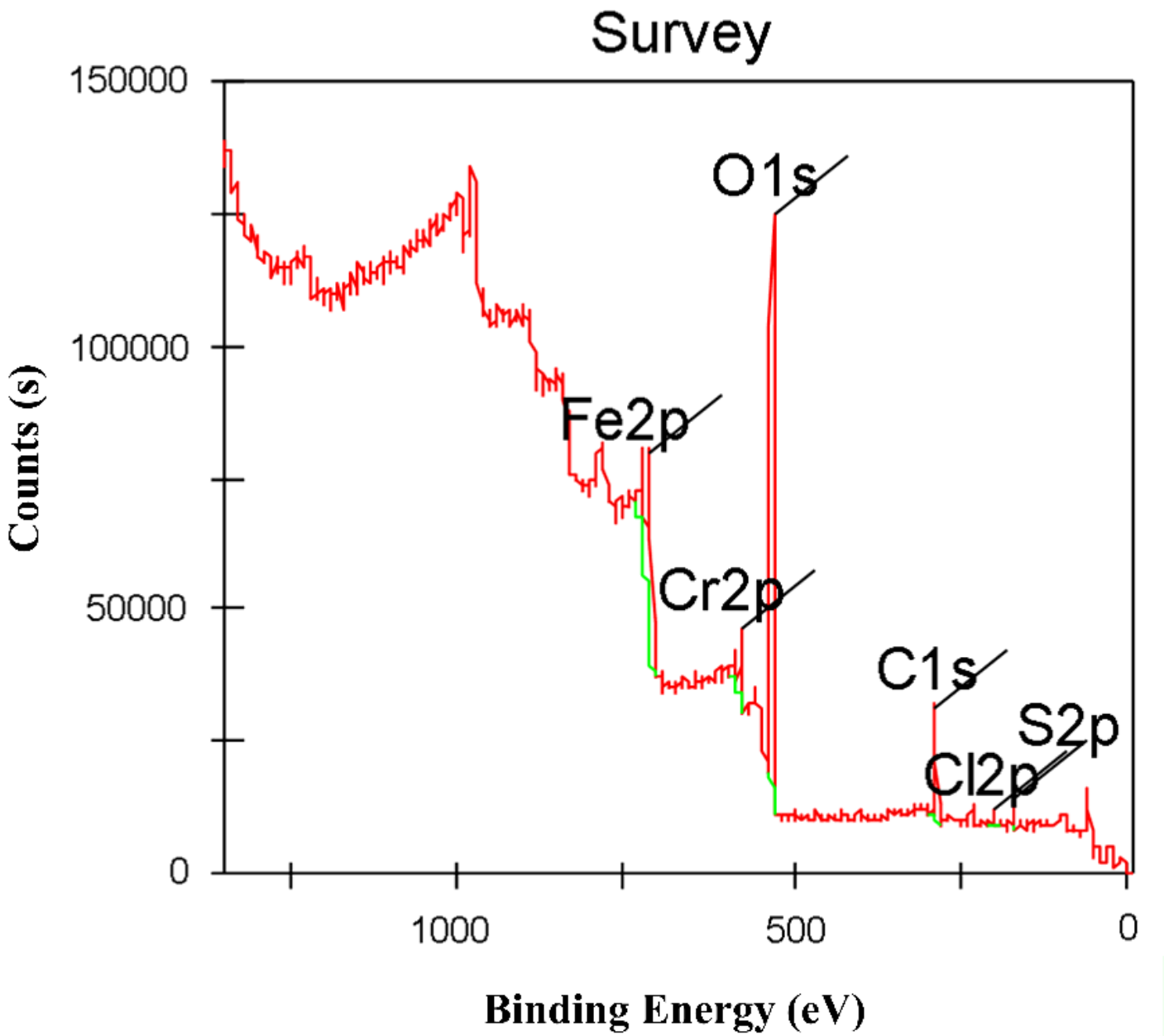

Figure 8

XPS wide survey of Cu/Fe bimetallic nanoparticles after removal reaction with Cr(VI) To further analyze the chemical compositions of Cr and Fe, detailed XPS spectra for Cr 2p and Fe 2p were carried out (Fig. 9 and Fig. 10). The Cr 2p3/2 and Cr 2p1/2 photoelectron peaks at 577.0 eV and 586.8 eV represent the binding energies of Cr(OH)3, Cr(OH)O, and Cr2O3. [40, 51, 52].

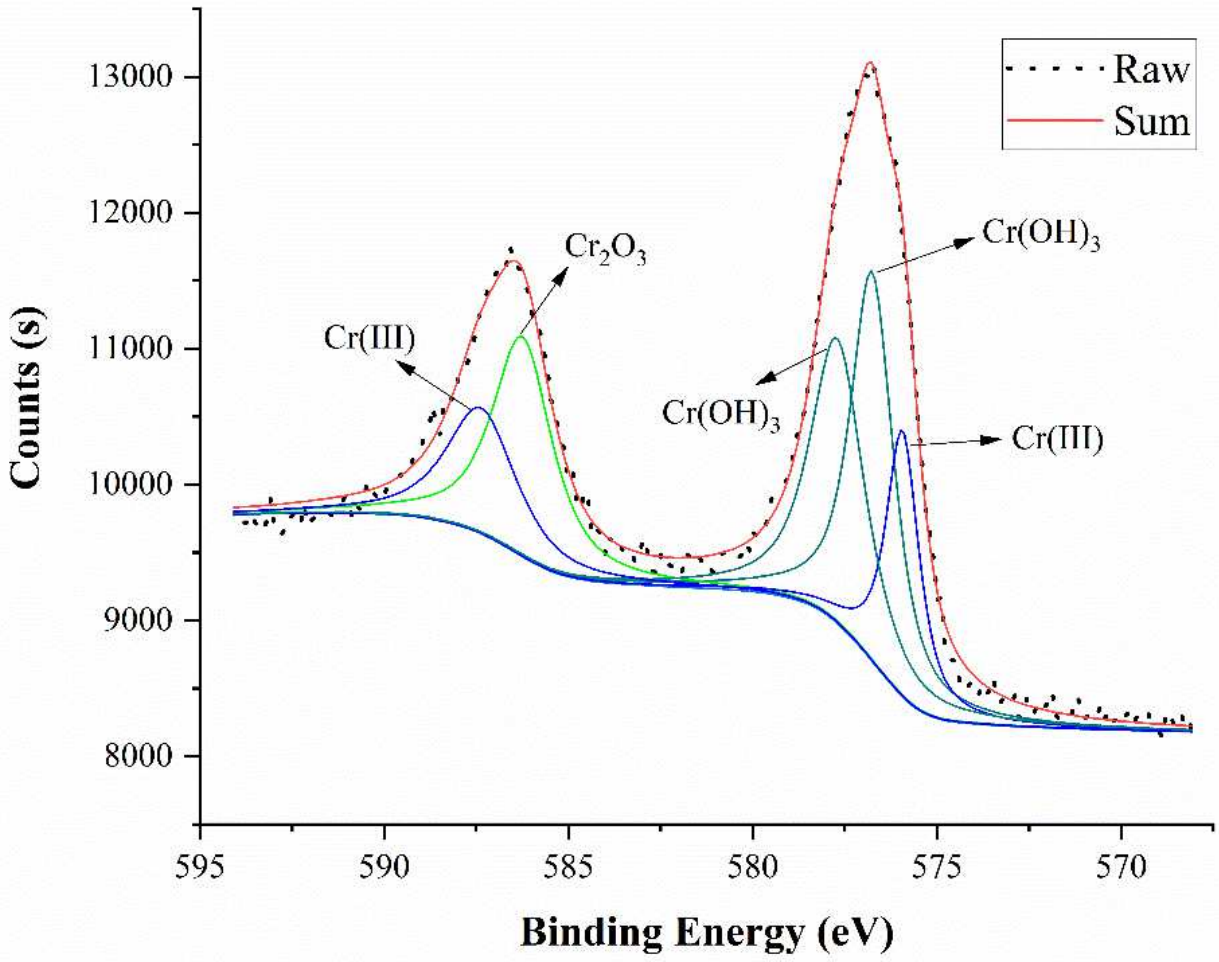

Figure 9

Cr2p XPS spectra of Cu/Fe bimetallic nanoparticles after removal reaction with Cr(VI)

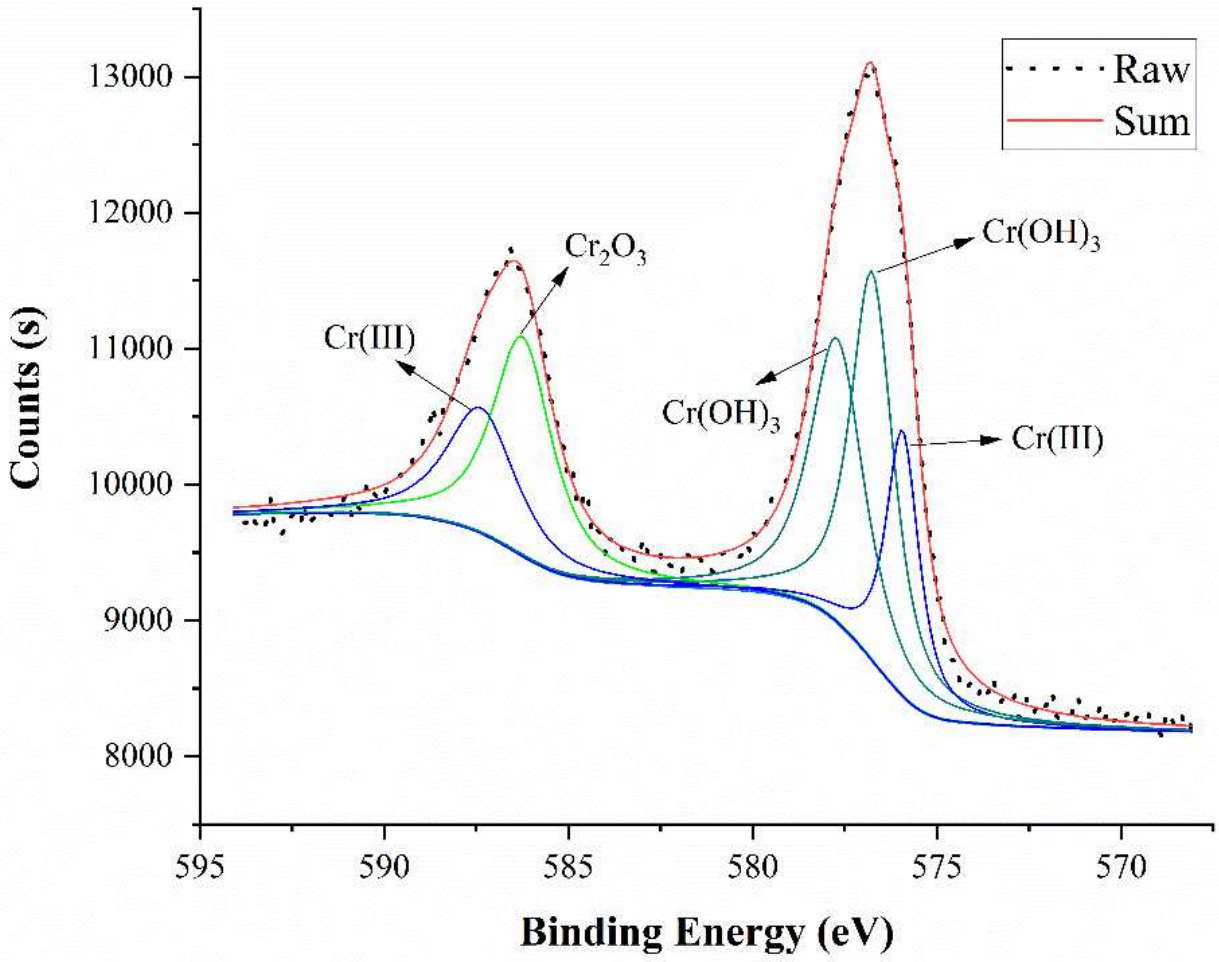

Figure 9

Cr2p XPS spectra of Cu/Fe bimetallic nanoparticles after removal reaction with Cr(VI)

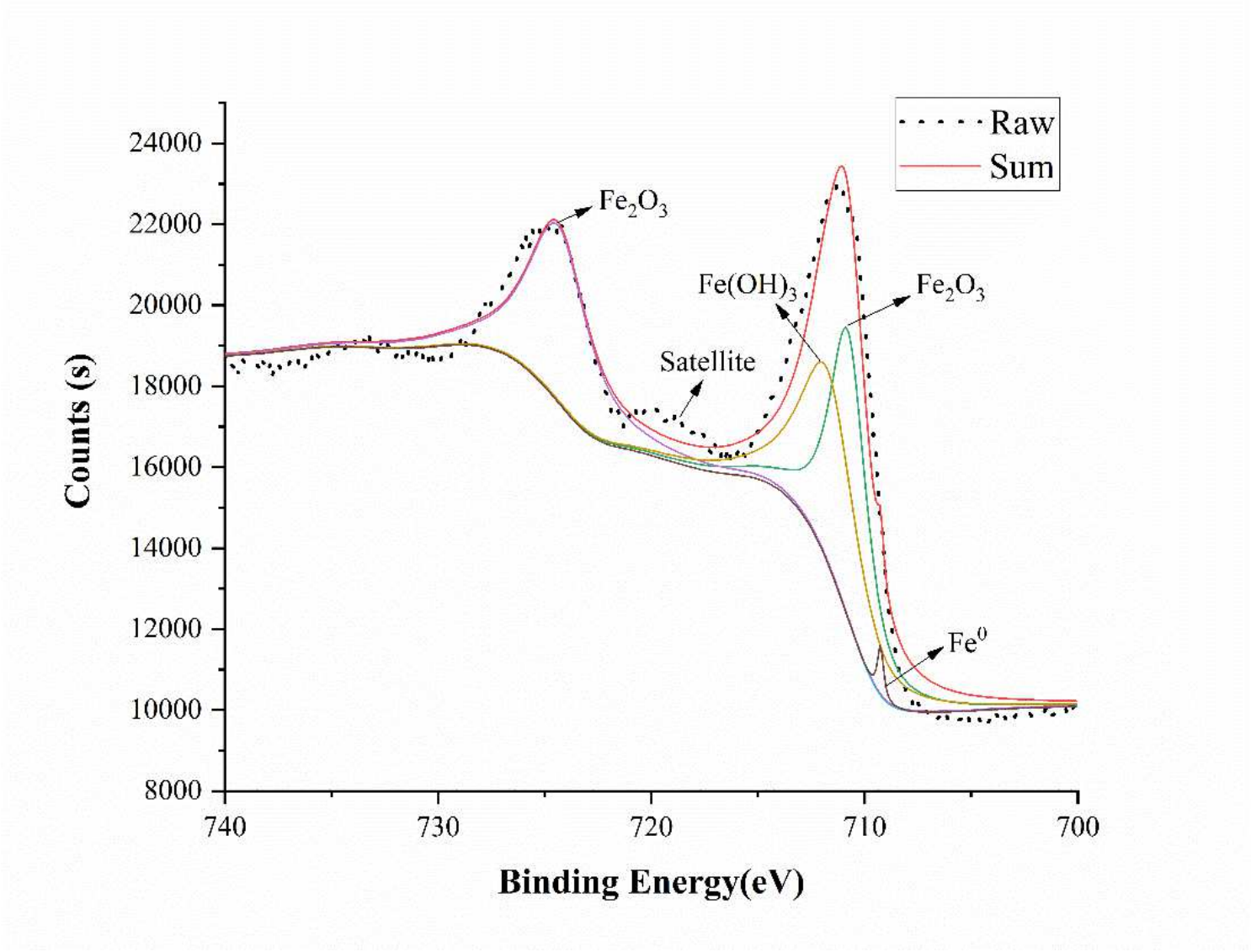

Figure 10

Fe2p XPS spectra of Cu/Fe bimetallic nanoparticles after removal reaction with Cr(VI)

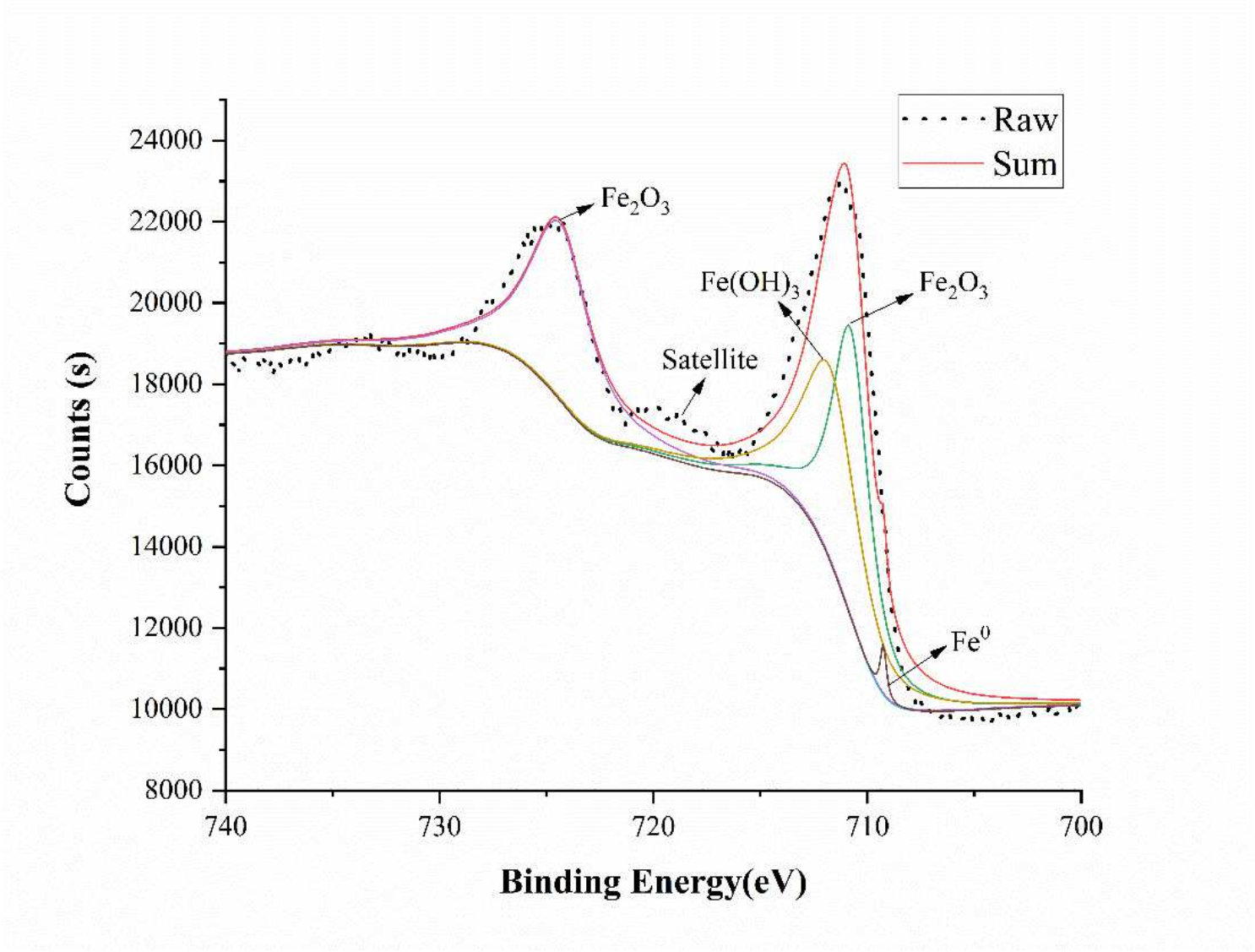

Figure 10

Fe2p XPS spectra of Cu/Fe bimetallic nanoparticles after removal reaction with Cr(VI)

Supplementary Files

This is a list of supplementary files associated with this preprint. Click to download.

- SupplementalInformation1130.docx
- SupplementalInformation1130.docx